Open access • Journal Article • DOI:10.1007/S00126-015-0598-8

Mobility of Au and related elements during the hydrothermal alteration of the oceanic crust: implications for the sources of metals in VMS deposits — Source link

Clifford Patten, Iain K. Pitcairn, Damon A. H. Teagle, Michelle Harris

Institutions: Stockholm University, National Oceanography Centre, Southampton

Published on: 01 Feb 2016 - Mineralium Deposita (Springer Berlin Heidelberg)

Topics: Oceanic crust, Volcanogenic massive sulfide ore deposit, Hydrothermal circulation, Basalt and Mafic

Mobility of Au and related elements during the hydrothermal alteration of the oceanic crust: implications for the sources of metals in VMS deposits.

Clifford GC Patten*[1], Iain K Pitcairn[1], Damon AH Teagle[2], Michelle Harris[2]

*Corresponding author: clifford.patten@geo.su.se; +46 (0)8 16 47 37

[1]Department of Geological Sciences, Stockholm University, Stockholm, SE-106 91, Sweden

[2]Ocean and Earth Science, National Oceanography Centre Southampton, University of Southampton, SO14-3ZH, United Kingdom

Abstract

Volcanogenic Massive Sulphide (VMS) deposits are commonly enriched in Cu, Zn and Pb and can also be variably enriched in Au, As, Sb, Se and Te. The behaviour of these elements during hydrothermal alteration of the oceanic crust is not well known. Ocean Drilling Program (ODP) Hole 1256D penetrates a complete in-situ section of the upper oceanic crust providing a unique sample suite to investigate the behaviour of metals during hydrothermal alteration. A representative suite of samples was analysed for Au, As, Sb, Se and Te using low detection limit methods, and a mass balance of metal mobility has been carried out through comparison with a fresh Mid-Oceanic Ridge Basalt (MORB) glass database. The mass balance shows that Au, As, Se, Sb, S, Cu, Zn and Pb are depleted in the sheeted dyke and plutonic complexes with mobilities of -46±12 %, -27±5 %, -2.5±0.5 %, -27±6 %, -8.4±0.7 %, -9.6±1.6 %, -7.9±0.5 % and -44±6 % respectively. Arsenic and Sb are enriched in the volcanic section due to seawater-derived fluid

circulation. Calculations suggest that large quantities of metal are mobilised from the oceanic crust but only a small proportion is eventually trapped as VMS mineralisation. The quantity of Au mobilised and the ratio Au to base metals are similar to that of mafic VMS and a ten times enrichment of Au would be needed to form a Au-rich VMS. The Cu-rich affinity of mafic VMS deposits could be explained by base metal fractionation both in the upper sheeted dykes and during VMS deposit formation.

Keywords: VMS deposit, Au-rich VMS, ODP Hole 1256D, hydrothermal alteration in the oceanic crust

Introduction

Volcanogenic Massive Sulphide (VMS) deposits are formed from hydrothermal mobilisation of metals in the oceanic crust (e.g. Schiffman et al. 1987; Richardson et al. 1987; Barrie and Hannington 1999). It is generally accepted that the metals enriched in these deposits, particularly those from ridge-related settings, were partly leached from deeper levels in the oceanic crust itself during hydrothermal alteration. For example, Ocean Drilling Program (ODP) drill cores from Holes 1256D and 504B in the Pacific Ocean show that S, Cu and Zn are depleted from the lower sheeted dykes and from the plutonic complex relative to the upper volcanic sections of the crust (Alt et al. 1989; Alt 1995; Teagle et al. 2006; Alt et al. 2010). Ophiolitic exposures of oceanic crust such as at Troodos in Cyprus also reveal large areas of hydrothermally altered rocks that are depleted in base metals (Richardson et al. 1987; Schiffman et al. 1987; Schiffman and Smith 1988; Jowitt et al. 2012). The areas of epidosite alteration that characterise the lower parts of the sheeted dyke complex at Troodos are systematically depleted in Cu, Zn, Ni and Mn relative to unaltered rocks (Jowitt et al. 2012). These depletions observed in the modern

44 day oceanic crust and in the ophiolitic section are considered to represent the source areas for the
45 metals enriching the VMS deposits that occur in these regions (e.g. Alt et al. 1989; Jowitt et al.
46 2012).

47 VMS deposits have high concentrations in the base metals Cu, Zn and Pb (e.g. Galley et
48 al. 2007; Mudd et al. 2013) but can also be enriched in Au, Ag, As, Sb, Se, Te and Bi. Deposits
49 enriched in the latter group of elements may be sub-classified depending on the degree of Au
50 enrichment into auriferous, anomalous and Au-rich VMS deposits (Mercier-Langevin et al.
51 2011), with the Au-rich deposits defined by a grade of more than 3.46 g/t Au and 31 t Au
52 (Mercier-Langevin et al. 2011) or by Au (ppm) > Cu+Zn+Pb (wt.%; e.g. Hannington et al. 1999;
53 Huston 2000). They account for a significant part of global Au production (e.g. 13 % in Canada,
54 80 % in Sweden; Mercier-Langevin et al. 2011). Despite the economic significance, the complex
55 and variable mechanisms leading to the enrichment of Au, As, Sb, Se and Te (hereafter referred
56 to as Au and related elements) are not well understood. The processes proposed to explain the
57 enrichment in Au and related elements include 1) sub-seafloor boiling in a shallow water
58 environment which changes the fluid chemistry causing enrichment of Au in a gas-rich fluid
59 (Urabe et al. 1987; Huston and Large 1989; Butterfield et al. 1990; Poulsen and Hannington
60 1996; Hannington et al. 1999), 2) formation in regions that contain high source area Au
61 concentrations such as in back-arc settings (Huston 2000; Moss et al. 2001; Pitcairn 2011) or
62 mantle plumes (Webber et al. 2013); and 3) input of Au and related elements from a magmatic
63 source such as shallow sub-seafloor intrusions (e.g. Urabe et al. 1987; Stanton 1990, Sillitoe et al.
64 1996).

65 Although mobility of base metals during alteration of the oceanic crust is relatively well
66 documented, very little is known about the effects of hydrothermal alteration on Au and related

elements (Keays and Scott 1976; Nesbitt et al. 1987; Korobeynikov and Pertsev 1995). For example, Nesbitt et al. (1987) reported mobility of Au from the sheeted dykes during hydrothermal alteration of ODP Hole 504B in the Nazca plate. However, a similar study from ODP Hole 504B but using a different analytical method showed no such mobility (Korobeynikov and Pertsev 1995; Korobeynikov and Pertsev 1996). There have been no reports of the behaviour of As, Sb, Se and Te during hydrothermal alteration in the oceanic crust. Systematic investigation of the behaviour of Au and related elements during hydrothermal alteration of the oceanic crust would greatly improve our understanding of the source area processes that generate Au-bearing fluids in the VMS environment.

ODP Hole 1256D in the Cocos Plate, Pacific Ocean is an ideal location to investigate these processes. The Hole 1256D drill core is unique in being the only core to sample a complete section of oceanic crust down to the plutonic complex (Teagle et al. 2006; Wilson et al. 2006). The alteration in Hole 1256D resulting from fluid circulation is well described (Teagle et al. 2006; Alt et al. 2010; Alt and Shanks 2011), providing a solid framework for investigation of the mobility of Au and related elements. In this study we investigate the behaviour of Au, As, Sb, Se, Te and S, as well as base metals Cu, Zn and Pb, during the hydrothermal fluid circulation in the oceanic crust sampled by Hole 1256D. We use low detection limit analytical methods for quantification of Au and related elements (Pitcairn et al. 2006a; 2006b). The objectives of the study are to quantify the mobility of Au and related elements and constrain their behaviour during the alteration of the oceanic crust. The results of the study provide significant insight into source areas for metals and the trapping efficiency of metals during formation of VMS deposits, particularly those that are Au-rich.

Geological setting

1. ODP Hole 1256D lithologic units:

ODP Hole 1256D is located in the Cocos Plate (6.736° N, 91.934° W), in a 15 Myr old crust that was generated at the East Pacific Rise during an episode of superfast spreading (~200 mm/yr; Wilson et al. 2003). Basement oceanic crustal material was recovered during four drilling cruises: ODP Leg 206 and IODP Expeditions 309/312 and 335 (Wilson et al. 2003; Teagle et al. 2006; Teagle and Harris 2011). Underlying 250 m of pelagic sediment, the oceanic crust at Site 1256 can be divided into four main lithological units: the volcanic section, transitional zone, sheeted dyke complex and plutonic complex (Figure 1).

The volcanic section extends down to 1004 meters below seafloor (mbsf), and comprises an upper section of lava ponds and inflated flows that were formed during off-axis volcanic events, and a lower section of phyric to aphyric sheeted flows and generally aphyric massive units (Wilson et al. 2003; Teagle et al. 2006). Below the volcanic section, the transitional zone extends from 1004 mbsf down to 1061 mbsf and is mainly composed of aphyric sheeted flows with sulphide-mineralised breccias at 1028 mbsf (Teagle et al. 2006). The mineralised breccias at 1028 mbsf are composed of angular aphyric cryptocrystalline basaltic clasts cemented by chalcedony, saponite, carbonate, albite, anhydrite and sulphides (Teagle et al. 2006). The sheeted dyke complex extends from 1061 mbsf to 1407 mbsf and comprises massive aphyric basalt (Teagle et al. 2006) with common sub-vertical intrusive contacts. In the lower part, the dykes have granoblastic textures formed by high-temperature recrystallization due to intrusion of the underlying gabbros (Teagle et al. 2006; Koepke et al. 2008). At the bottom of the hole two gabbro bodies intrude the sheeted dykes. The upper gabbro is characterised by gabbros, oxide gabbros, quartz-rich oxide diorites and small trondhjemite dykelets (Teagle et al. 2006; Koepke et

al. 2008). The lower gabbro body consists of medium-grained gabbro-gabbronorite with minor trondhjemite dykelets. The contacts between the gabbro bodies and the dykes are intrusive with dyke fragments occurring in the margin of the lower gabbro body (Teagle et al. 2006; Alt et al. 2010).

2. Hydrothermal system:

The Hole 1256D oceanic crust preserves a complex history of hydrothermal fluid flow. Two main domains of fluid flow have been identified: an upper seawater-derived fluid domain and a lower hydrothermal fluid domain (Teagle et al. 2006, Alt et al. 2010). The seawater-derived domain occurs mostly in the volcanic section and the transitional zone and is characterised by alteration formed from circulation of low-temperature (<50°C-185°C; Fig.1) oxidised fluids (Alt et al. 2010; Coggon et al. 2010). The most common alteration style is relatively low intensity background alteration (2-20 % recrystallisation) where the primary mineralogy is partially replaced with saponite, celadonite, iron oxyhydroxides, chalcedony and minor pyrite, giving the rocks a more greyish colour (Wilson et al. 2003; Teagle et al. 2006; Alt et al. 2010). The intensity of alteration is controlled by the permeability which is a function of the lava morphology and the distribution of breccias and fractures (Teagle et al. 2006). Massive flows act as impermeable barriers and fluid flow is channelled along their margins (Harris et al. 2015). An example of the alteration caused by this channelled fluid flow occurs at 648 mbsf where an intensively altered 80 cm interval referred to as the "red brick horizon" is recrystallised to celadonite, saponite, K-feldspar, chlorite and quartz (Harris et al. 2015). Veins with intensely altered black and brown alteration halos are common in the volcanic section. The black alteration halos, containing mainly celadonite, are suggested to have been formed by early low-temperature alteration under anoxic conditions (Teagle et al. 2006). The brown alteration halos, characterised by iron oxyhydroxides

and iron-rich saponite and commonly exhibiting a disseminated pyrite front external to the halo, are interpreted to have formed during the flow of cold oxidising seawater (Alt et al. 2010).

The hydrothermal fluid domain occurs in the sheeted dyke complex and the plutonic rocks and is characterised by alteration formed from circulation of high-temperature (300°C to >650°C; Fig. 1) reduced fluids (Alt et al. 2010). The background alteration of the rocks is pervasive and gives a light to dark green colour (Teagle et al. 2006). Secondary minerals include chlorite, actinolite, albite, titanite and pyrite, which correspond to sub-greenschist and greenschist facies conditions (Teagle et al. 2006; Alt et al. 2010). Below 1300 mbsf actinolite is more common than chlorite, indicating an increase in the temperature of alteration. The intensity of alteration tends to be higher in the vicinity of veins forming dark green halos. Additionally, veins of quartz, chlorite, epidote, pyrite, chalcopyrite, magnetite and rare sphalerite overprint the background alteration and have been interpreted to represent hydrothermal fluid precipitates (Alt et al. 2010). Fluid flow in the sheeted dyke complex is preferentially channelled along dyke margin (Harris 2015). Below 1348 mbsf the granoblastic dykes are recrystallised to secondary clinopyroxene, orthopyroxene, actinolitic hornblende, plagioclase, magnetite and ilmenite (Teagle et al. 2006; Koepke et al. 2008). Alteration of the gabbro is controlled by grain size, with coarse-grained rocks tending to be more intensely altered.

The upper seawater-derived and lower hydrothermal fluid domains overlap and interact in the lava-dyke transitional zone unit. Here, alteration assemblages preserve a very steep thermal step over a short vertical distance from lavas altered at low temperature alteration and rocks partially recrystallised to greenschist facies assemblages. The transitional zone is a region of interaction between down-welling seawater-like fluids and up-welling hydrothermal fluids; this mixing has resulted in the precipitation of anhydrite, pyrite, sphalerite, and minor chalcopyrite

158 veins. A 2.8 m-wide section of quartz-sulphide-mineralised hyaloclastic breccia, where the main
159 sulphides are pyrite, sphalerite and minor chalcopyrite, occurs in this unit (Teagle et al. 2006; Alt
160 et al. 2010).

161 ## Sampling and analytical methods

162 Rock chips and powdered rock samples from the Hole 1256D drill core were prepared at
163 the National Oceanographic Centre Southampton (NOCS). A suite of 63 samples distributed
164 along the whole length of the hole (from 261 mbsf to 1495 mbsf, Fig. 1), representative of the
165 variation in lithology and the style and intensity of alteration, was selected. Gold analyses were
166 carried out at Stockholm University using a Thermo XSeries 2 ICP-MS following the ultra-low
167 detection limit method described in Pitcairn et al (2006a). The 3σ method detection limit is 0.033
168 ppb Au. Analytical precision for Au analyses at Stockholm University was controlled through
169 analyses of CANMET reference material TDB1 and USGS reference materials WMS-1, CH-4
170 and BIR-1 (Table 1). Arsenic, Sb, Se and Te analyses were also carried out at Stockholm
171 University by Hydride Generation-Atomic Fluorescence Spectrometry (HG-AFS) using a PSA
172 10.055 Millennium Excalibur instrument following the method described in Pitcairn et al.
173 (2006b). Analyses were carried out on the same acid digests as those used for Au analyses. The
174 3σ instrumental detection limits are 0.043 ppb, 0.079 ppb, 0.038 ppb, and 0.22 ppb for As, Sb, Se
175 and Te, respectively. Reference materials TDB-1, WMS-1 and CH-4, along with our internal
176 reference sample BAS 206, were used to control analytical precision and accuracy (Table 1).

177 Sulphur, Cu, Zn, Pb, major and trace elements data are reported in Harris (2011). Samples
178 were analysed for major and trace elements concentration by X-ray fluorescence spectrometry
179 (XRF) using Phillips PW2404 automatic X-Ray Spectrometers at the University of Leicester

(ODP 206 samples) and at the University of Edinburgh (IODP Expedition 309/312 samples) following the methods of Harvey (1989) and Fitton et al. (1998), respectively (see Harris, 2011 for details). Sulphur contents were determined using a LECO CS 225 CS-analyser at the University of Leicester. Lead analyses were carried out by ICP-MS using a Thermo Fisher X-series Mk II at the University of Southampton. Precision and accuracy were estimated through analyses of international reference materials of BIR-1, BHVO-1 and BCR-1 for Cu and Zn with values similar to those reported in Fitton et al. (1998); BAS ECRM 877-1 was used for S and BIR-1 and BHVO-2 for Pb (Table 1).

Whole-rock results

The distribution of Au and related elements in Hole 1256D is shown in Figures 2 and 3, the distribution of S and base metals in Figure 4, and all data is reported in Appendix 1. The sample populations have a positively skewed distribution due to a small number of samples with very high concentrations. These samples are mostly located in the transitional zone and correspond to sulphide-rich mineralisation formed from the mixing of rising hydrothermal fluids with cold seawater-derived fluids (Teagle et al. 2006; Alt et al. 2010; Harris et al. 2015). All elements show the highest concentrations in the transitional zone except for Cu, which has the highest concentrations in the upper sheeted dyke section. In groups of samples from different sections of the hole, the positively skewed distribution is highlighted by a discrepancy between the arithmetic mean and the median for each element. We report the range of values, the arithmetic mean (referred to below as the mean) and the median for all elements. The standard deviation is not reported when it is higher than the arithmetic mean. The median concentration of Au (0.30 ppb) in Hole 1256D is similar to the median Au value of fresh MORB glass estimated

by Webber et al. (2013; 0.34 ppb, n=22). Median concentrations of As, Sb, Se, S, Cu, Zn and Pb (74 ppb, 27 ppb, 200 ppb, 0.11%, 81 ppm, 96 ppm and 0.26 ppm, respectively) are also similar to that of average MORB (110 ppb, 14 ppb, 200 ppb, 0.11 %, 70 ppm, 80 ppm and 0.26 ppm, respectively; Arevalo and McDonough 2010). The median value of Te (23 ppb) is higher than the average fresh MORB value of 5 ppb Te estimated by Yi et al. (2000). In the volcanic section, Au, As, Sb, Se and S are affected by the variable style of low temperature alteration causing a large variation in concentrations. Tellurium, Cu, Zn and Pb are less strongly affected by low temperature alteration and show more homogeneous distributions (Fig 2 and 4). In the sheeted dyke and plutonic complexes, Au, As, Se, S, Cu show decreasing concentrations with depths from ~1100 mbsf and downward. Concentrations of Zn and Pb also decrease with depth, but from slightly deeper levels (~1200 mbsf), and Sb and Te show no systematic variation in content in these two units. Within the plutonic complex there is no apparent systematic difference in concentrations between the upper gabbro, the sheeted dyke screen and the lower gabbro for the elements investigated.

Gold:

The Au concentrations in Hole 1256D range from 0.05 to 8.2 ppb with mean and median values of 0.49 ppb and 0.30 ppb respectively (Figs. 2 and 3; Appendix 1). In the volcanic section, the red brick horizon has the lowest Au concentrations (0.07 to 0.1 ppb) whereas the brown and black alteration halos and the breccia samples have relatively high Au concentrations (0.7 to 2.1 ppb). Samples affected by the background alteration in the volcanic section have a relatively heterogeneous distribution with mean and median Au concentrations of 0.47±0.45 ppb and 0.35 ppb respectively. The highest Au concentrations in sulphide mineralised breccia from the transitional zone are up to 8.2 ppb Au. Samples affected only by background alteration in the

225 sheeted dyke and the plutonic complexes have mean and median concentrations of 0.20±0.12 ppb
226 and 0.20 ppb respectively, showing homogeneous distribution but decreasing content with depth
227 (Figs. 2 and 3; Appendix 1).

228 Arsenic:

229 Arsenic concentrations in Hole 1256D range from 17 ppb to 18.2 ppm with mean and
230 median values of 520 ppb and 74 ppb respectively. Samples affected by the background alteration
231 in the volcanic section show homogeneous distribution with mean and median As concentrations
232 of 114±66 ppb and 108 ppb respectively. Samples with specific alteration (e.g. black and brown
233 halos) have higher As concentrations up to 432 ppm (Figs. 2 and 3; Appendix 1). In the
234 transitional zone the sulphide-mineralised samples show up to 18.2 ppm As; samples from the
235 transitional zone that are affected by the background alteration also have high As concentrations
236 (up to 4.5 ppm). In the sheeted dyke and the plutonic complexes, samples affected only by
237 background alteration have mean and median As concentrations of 72±42 ppb and 64 ppb
238 respectively (Fig.2; Appendix 1); in the upper sheeted dykes sulphide-bearing samples in veins or
239 breccia show the highest concentration in these units.

240 Antimony:

241 The Sb concentrations in Hole 1256D drill core range from 8.2 to 592 ppb with mean and
242 median values of 45 ppb and 27 ppb, respectively. In the volcanic section, samples affected by
243 the specific low temperature alterations have higher concentrations than background altered
244 samples, which have an average concentration of 29±12 ppb (Figs. 2 and 3; Appendix 1).
245 Antimony concentrations in the sheeted dyke and plutonic complexes show little variation with
246 an average concentration of 24±8 ppb and no clear variation with depth.

247 Selenium:

248 The Se concentrations in Hole 1256D range from 3.9 ppb to 2.7 ppm with mean and
249 median values of 315 ppb and 200 ppb, respectively. The red brick horizon at 648 mbsf has very
250 low Se concentrations (8.6 to 30 ppb), whereas the brown alteration halos are relatively Se-rich
251 (Figs. 2; Appendix 1). The samples with background alteration in the volcanic section show
252 homogeneous distribution with mean 217±69 ppb Se. Selenium concentrations in the mineralised
253 breccias and sulphide-rich samples are up 2.6 ppm. In the sheeted dyke and the plutonic
254 complexes Se shows a wide concentration range, from 3.9 ppb up to 2.7 ppm, and a marked
255 decreasing trend with depth. In the upper sheeted dykes high concentration samples are sulphide-
256 bearing, similar to those of the transitional zone (Fig. 2).

257 Tellurium:

258 Tellurium concentrations in Hole 1256D range from 8.3 to 92 ppb with mean and median
259 values of 26±14 ppb and 23 ppb respectively (Figs. 2 and 3; Appendix 1). Unlike the other
260 elements, Te has a very homogenous distribution with values varying by only one order of
261 magnitude. In the volcanic section the background alterated samples have a mean Te
262 concentration of 25±8.6 ppb (Figs. 2 and 3). In the sheeted dyke complex the mean Te
263 concentrations is 26±14 ppb, which is similar to the plutonic complex mean of 24±11 ppb (Figs.
264 2 and 3; Appendix 1).

265 Sulphur and base metals:

266 Sulphur and base metal concentrations for the Hole 1256D drill core have been previously
267 investigated, but using a different sub-set of samples to this study (Alt et al. 2010; Alt and Shanks
268 2011). Sulphur and base metal concentrations in Hole 1256D are shown in Figure 4. The median
269 S concentration (0.11 wt.%) is similar to average fresh MORB of 0.11 % (Arevalo and

McDonough 2010) but higher than that mean measured by Alt and Shanks (2011) of 528±342 ppm for the Hole 1256D volcanic section. In the volcanic section the S concentrations are strongly affected by the variable styles of alteration (Fig. 4, Alt and Shanks 2011) but background altered samples have a mean value of 0.11±0.08 wt.% S. Copper, Zn and Pb show little variation in the volcanic section, with mean values of 81.1±14.3 ppm, 98.1±18.3 ppm and 0.37±0.20 ppm, respectively, and are less affected by variable styles of alteration except in the red brick horizon, where they all show the lowest concentrations. In the sheeted dyke and plutonic complexes the S, Cu, Zn and Pb show wide ranges of concentrations and have median values of 0.12 wt. %, 76.9 ppm, 99.4 ppm and 0.23 ppm, respectively (Fig. 4; Appendix 1). Similarly to Au, As and Se, the highest S, Cu, Zn and Pb concentrations are in brecciated or sulphide-bearing samples within these two units.

Discussion

Primary metal contents:

The distribution of Au and related elements in the different lithological units of the Hole 1256D drill core suggests that they have been variably mobilised by hydrothermal alteration. To quantify the degree of mobility, the primary concentrations of Au and related elements prior to hydrothermal fluid circulation must be determined. A suite of nine least-altered samples from the volcanic section selected on criteria that include the preservation of spherical magmatic sulphides, K_2O concentrations ≤0.11 % and $^{87}Sr/^{86}Sr$ close to basalt values (Harris et al. 2015), combined with fresh glass values from Geldmacher et al. (2013), provides an estimate of the primary metal contents of the Hole 1256D crust (Table 2). However, these values may not be a true indication of the primary metal contents because 1) these samples are still slightly altered,

292 which may have affected the original metal concentrations, and, 2) the primary metal contents of
293 the rocks in the Hole 1256D crust may have varied, as it was generated by more than one
294 magmatic episode and has undergone varying degrees of magmatic fractionation (Teagle et al.
295 2006; Sano et al. 2011).

296 We assume that the intrusive gabbros in the plutonic section and the near off-axis lava
297 flows that comprise the upper part of the volcanic section were generated from a melt source with
298 a generally similar primary composition to that which produced the main volcanic and sheeted
299 dyke sections of the Hole 1256D crust (Teagle et al. 2006). The main compositional variation in
300 the Hole1256D oceanic crust is most likely to be due to magmatic fractionation (Teagle et al.
301 2006; Sano et al. 2011). In order to assess the behaviour of Au and related elements during
302 fractionation, metal concentrations from a large number of fresh glass samples from Pacific
303 Ocean spreading ridges are used (Jenner and O'Neill 2012). Samples from the Jenner and O'Neill
304 (2012) database are selected based on the following criteria: 1) samples are from Pacific Ocean
305 spreading centres and, 2) samples with anomalously high K_2O concentrations that have most
306 likely been affected by seawater alteration are not used. Immobile element concentrations of the
307 selected samples are indicative of fresh MORB compositions that have not been affected by
308 alteration (Pearce and Cann, 1973; Appendix 2). The behaviour of Au and related elements
309 during fractionation can be observed by plotting the element of interest against Y, which is used
310 as a proxy for magmatic fractionation (Figs. 5 and 6; Jowitt et al., 2012). We have chosen Y
311 rather than Mg# or Ti because Y is magmatically incompatible, immobile during hydrothermal
312 alteration (Staudigel 2003), and not influenced by Fe-Ti-oxide saturation during differentiation
313 (Jowitt et al. 2012). A series of differentiation curves have been plotted using the following
314 relationship from Jowitt et al. (2012):

315 $$E_e = AY^B \quad [1]$$

316 where Ee is the estimated element concentration for a given Y concentration and A and B are
317 regression coefficients (Table 3). Errors on differentiation curves are calculated using the Root
318 Mean Square Deviation (RMSD, Table 3). In order to have differentiation curves specific to Hole
319 1256D samples, the curves determined using Jenner and O'Neill (2012) database are centred on
320 the primitive compositions estimated in Table 2 (Fig. 5 and 6, Table 3). All elements show strong
321 trends with Y indicating that their concentrations are affected by magmatic fractionation (Figs. 5
322 and 6). Due to its strong chalcophile nature, Te is a compatible element during differentiation (Yi
323 et al. 2000; Patten et al. 2013); however, no database of fresh glass from Pacific Ocean spreading
324 ridges are known to the authors, preventing the calculation of a differentiation curve for Te.

325 Mass balance:

326 Mass balance calculations are carried out from the differentiation curves using the method
327 described by Jowitt et al. (2012):

328 $$\%\ \text{Change} = (E_s - E_e)/\ E_e * 100 \quad [2]$$

329 where E_s is the measured value from the samples and E_e the estimated primary crust composition
330 from equation [1]. Mass change calculations are only relevant if Y concentrations have remained
331 constant during alteration. Large additions or removal of mass during alteration could cause
332 residual dilution or concentration of Y. Jowitt et al. (2012) used the mass variation of Al_2O_3 as a
333 proxy for bulk mass changes during alteration of the rock. Both Al_2O_3 and Y are immobile during
334 alteration, but they behave differently during magmatic differentiation as Y is incompatible
335 whereas Al_2O_3 is compatible. A discrepancy between the measured and estimated Al_2O_3
336 concentrations will therefore indicate whether there have been mass changes during alteration

337 (Jowitt et al. 2012). The estimated Al_2O_3 concentration in Hole 1256D for a given Y value is
338 estimated using the following equation:

339 $$Al_2O_3(\text{wt.}\%) = 29.298 * Y^{-0.214} \quad [3]$$

340 determined using the Jenner and O'Neill (2012) database and the primary Al_2O_3 concentration
341 (13.8 wt.%) from the least altered samples (Table 2). The average mass variation of Al_2O_3 in
342 Hole 1256D samples calculated from equation [3] is -2.46 % (i.e. -0.34 wt.% Al_2O_3), which is
343 similar to the RMSD of 2.31 % indicating that relatively little mass change affected the samples.
344 The Y concentrations in Hole 1256D can thus be considered to have remained constant in the
345 rock during alteration and to be a suitable proxy to determine primary crust composition through
346 magmatic differentiation.

347 As no differentiation curve could be calculated for Te, the mass variation is carried out
348 using the method described by Nesbitt (1979):

349 $$\text{Te \% Change} = \left(\frac{\text{Te}_{\text{sample}}}{Y_{\text{sample}}} * \frac{Y_{primary}}{\text{Te}_{primary}} - 1\right)*100 \quad [4]$$

350 where Te_{sample} and Y_{sample} are the concentrations of Te and Y in the sample, respectively,
351 and $Te_{primary}$ and $Y_{primary}$ are the concentrations of the primary crust estimated in Table 2. This
352 mass calculation, assuming that Te concentration is constant in the primary crust, is an
353 oversimplification. All elemental mass changes calculated are shown in Figures 7 and 8 and listed
354 in Table 4 for each unit. The error propagation for the mass balance calculations is described in
355 detail in Appendix 3. The main errors are caused by the heterogeneous distribution of the
356 chemical elements in the rocks, which can be estimated from the relative standard deviation of
357 preferred reference materials (Table 1) and the normalised RMSD (NRMSD) of the Jenner and
358 O'Neill (2012) database (Table 3). Errors on mass balance calculations vary from 8.5 % for S up

359 to 25.0 % for Au. Tellurium has high error (44.6 %) due to the poor constraint of protolith
360 concentrations.

361 Metal mobility in deep hydrothermal alteration zones:

362 In the sheeted dyke and plutonic complexes, where hydrothermal fluids are hot (>300 ºC;
363 Alt et al. 2010), almost all of the investigated elements have significantly lower concentrations
364 than primary crustal compositions, implying that they have been mobilised during hydrothermal
365 alteration (Figs. 7 and 8). In the sheeted dyke complex, sulphide-rich and brecciated samples,
366 present mostly in the upper sheeted dyke section represent local metal precipitation from the
367 hydrothermal fluids and do not represent the background altered samples. Metal depletions are
368 therefore calculated only from median values of background altered samples (Table 4). Although
369 few sulphide-rich samples are present in the plutonic complex, they are interpreted to be
370 associated with hydrothermally altered rocks and the median values of all samples are used for
371 metal depletion calculations. Gold and Pb are the most depleted elements in the sheeted dyke and
372 plutonic complexes (-46±11.5 % and -44.4±6.6 %, respectively) followed by As and Se (-
373 27.2±5.4 % and -26.7±5.7 %, respectively) and Cu, S, Zn and Sb (-9.6±1.9 %, -8.4±0.9 %, -
374 7.9±0.9 and -2.5±0.5 %, respectively); Te is the only element showing enrichment (13.7±5.7 %;
375 Table 5). This variation in depletion implies different solubility in the hydrothermal fluids in the
376 following order: Au~Pb>As~Se>S~Cu~Zn>Sb>Te, with Au being the most soluble and Te the
377 least. The Te enrichment could be an artefact of the mass balance calculation as an appropriate
378 differentiation curve could not be determined. The mass balance calculation for S is an
379 underestimate of the S mobilised by hydrothermal fluid circulation, as the whole rock S data
380 comprise S from anhydrite and from pyrite that formed by seawater sulphate reduction.

381 The range of Au, As and Sb concentrations in the sheeted dyke and plutonic complexes is
382 considerably lower than in the volcanic section, indicating that the deep high-temperature
383 hydrothermal alteration in the lower crust effectively leaches the rocks of these elements,
384 resulting in a more homogeneous distribution (Fig. 3). The depletion of Au is in the same order of
385 magnitude as that from Hole 504B, where a ~60 % loss of Au from greenschist altered rocks is
386 estimated (Nesbitt et al., 1987). Samples with high sulphide content either in the form of veins,
387 breccias or disseminated grains are enriched in all elements relative to the background altered
388 samples (Table 4), suggesting that sulphides play an important role on their distribution. Overall,
389 Au, As, Se, S, Cu, and Sb (and to a lesser extent Pb) show similar depletion patterns through the
390 sheeted dyke and the plutonic complexes being mobilised from below ~1100-1150 mbsf. Zinc,
391 however, shows a strikingly different depletion pattern. Although Zn is depleted overall in the
392 two units, it shows enrichment in the upper sheeted dykes and depletion in the lower sheeted
393 dykes and the plutonic complex. In the upper sheeted dykes both background altered and
394 sulphide-rich samples are enriched in Zn, implying that silicate phases and/or oxides also host Zn
395 (Doe, 1994). Sphalerite is a relatively common sulphide mineral in the upper sheeted dyke veins
396 but the data indicate that silicates such as chlorite, which is the most abundant secondary mineral
397 in the sheeted dykes, also host Zn. This is in agreement with previous work from the Troodos
398 ophiolite, which shows that in rocks altered by hydrothermal fluids, Zn can be hosted by Mg-
399 bearing minerals such as chlorite (Jowitt et al. 2012). Lead shows a generally similar depletion
400 pattern to Au, As, Se, S, Cu and Sb in the sheeted dyke and plutonic complexes, but it also shows
401 some enrichment in the upper sheeted dyke section (Fig. 8), suggesting some similarity in
402 behaviour with Zn. The enrichment of Zn in the upper sheeted dyke section implies that metal
403 fractionation occurs during metal transportation from the deep crust towards the seafloor, which
404 will affect the metal composition of the hydrothermal fluids from which VMS deposits are

generated. Mafic VMS deposits commonly have a Cu/Zn ratio of around 1.8 (e.g. Barrie and Hannington 1999), which is different from the ratio in fresh MORB source rock (fresh MORB Cu/Zn=0.9; Arevalo and McDonough 2010). This may be partly due to preferential trapping of Zn relative to Cu in the upper sheeted dyke section during hydrothermal fluid circulation.

Metal mobility in shallow seawater-dominated alteration zones:

Alteration in the volcanic section is controlled by circulation of low temperature seawater-derived fluids that cause both the background alteration and the brown and black halos. Alteration halos, veins and breccias make up ~6.5 % of the Hole 1256D drill core (Alt et al. 2010) and background altered samples the remaining 93.5 %. In the samples showing background alteration, As, Sb and Se are enriched relative to the protolith concentrations (20 %, 19.9 % and 13.8 %, respectively) whereas S is depleted (-10.5 %); the other elements do not show significant variation (<±10 %, Table 4). Alt and Shanks (2011) suggested that S loss from the volcanic section was due to degassing at eruption. Alteration halos and brecciated samples show strong enrichment in Au, As and Sb and depletion in Pb (Table 4). Taking into account the relative proportions of background alteration and vein halos, the mass variation in the volcanic section as a whole shows that As, Sb and Se are enriched (30.4 %, 24.5 % and 12.7 %, respectively), whereas other elements do not show significant variation (<±10 %, Table 4).

In the volcanic section, As and Sb show some correlation with K_2O and Rb (Fig. 9), indicating that they were added by seawater-derived fluid circulation. Specific alteration such as brown and black alteration halos are strongly enriched in As and Sb (Fig. 9, Table 4), implying that these elements are easily added in rocks that are more intensely altered by seawater-derived fluids. Mass variations in the red brick horizon are not calculated, but the elemental concentrations suggest that Au, Se, S, Cu, Zn and Pb were removed whereas Sb and most likely

As were added (Fig. 2 and 4). The red brick horizon is suggested to be a typical example of a pathway for channelled low temperature (~60 ºC, Alt et al. 2010) hydrothermal fluids in the volcanic section (e.g. Harris et al. 2015). The low concentrations of Au, Se, S, Cu, Zn and Pb in this horizon suggest that there was little precipitation of metals from the hydrothermal fluids during their circulation through the volcanic section.

The black and brown alteration halos are relatively scarce in the Hole 1256D crust and therefore do not contribute greatly to the mass balance. Seawater-derived fluid alteration is considered to be limited in Hole 1256D crust primarily due to fast sediment blanketing and the presence of a massive lava flow in the upper volcanic section, which sealed the oceanic crust from late seawater infiltration (Alt et al, 2010; Harris et al. 2015). Brown and black alteration halos are much more common in Hole 504B (Wilson et al. 2003) and it is likely that the volcanic section there is more strongly enriched in As and also in Sb. Elements such as As and Sb are amongst those shown to be released from subducting oceanic crust into the overlying mantle wedge during subduction (Hattori et al. 2005; Hattori and Guillot 2003). Sediments overlying the subducting slab may provide the bulk of the As and Sb released in the mantle wedge element but the volcanic section could be an important alternative source.

Gold is enriched in brecciated, brown altered and black altered samples but does not correlate with K_2O or Rb, suggesting that Au is not enriched by seawater-derived fluid circulation in the volcanic section. Nesbitt et al. (1987) showed that in Hole 504B volcanic section Au was not enriched but that redistribution did occur.

448 Metal behaviour in the transitional zone:

449 The transitional zone, where the seawater-derived fluid and hydrothermal fluid domains
450 meet in Hole 1256D, is characterised by zones of sulphide mineralisation (Teagle et al. 2006).
451 Relative to the primary crust, the sulphide-mineralised samples are strongly enriched in all the
452 elements investigated in this study, with the exception of Cu (Figs. 7 an 8 and Table 4). Whereas
453 Hole 504B hosts a quartz-epidote-pyrite-chalcopyrite mineralised stockwork (e.g. Alt et al.,
454 1996), the Hole 1256D mineralized breccia at 1028 mbsf appears to be a relatively low
455 temperature feature (Teagle et al. 2006; Harris et al. 2015), which may have prevented extensive
456 Cu precipitation. Copper mineralisation in Hole 1256D occurs at deeper levels in the sheeted
457 dykes (1090-1115 mbsf) as chalcopyrite-rich veinlets and breccias (e.g. Harris et al. 2015). In the
458 transitional zone, some of the elements, including As, Sb, Se and Pb, are also enriched in the
459 samples with background alteration (Figs. 7 and 8, Table 4), indicating that these elements might
460 also be incorporated into silicate or oxide minerals. The source of the metals locally enriched in
461 the transitional zone is interpreted to be the depletion zones observed in the underlying sheeted
462 dyke complex and plutonic complex. It is suggested that the mass of metals precipitated in the
463 transitional zone from the hydrothermal fluids represents only a fraction of the total quantity
464 present in the fluids; the majority of the metals mobilised are believed to be transported to the
465 seafloor (Nesbitt et al. 1987; Hannington et al. 1990; Alt et al. 2010). In other localities, however,
466 the transitional zone represents an important metal sink for the metals transported by
467 hydrothermal fluid (Coogan and Dosso 2012; Hannington 2013).

468 Implications for VMS formation

469 Mid-ocean ridge (MOR) VMS deposits are classified as “mafic deposits” (Barrie and
470 Hannington 1999). They have been reported to occur along all mid-ocean spreading ridges so far

471 investigated, including the East Pacific Rise, the Mid-Atlantic Ridge (e.g. TAG hydrothermal
472 field) and the Juan de Fuca Ridge (Herzig and Hannington 1995; Beaulieu 2010). They are
473 typically smaller in size than other classes of VMS deposits, ranging from ≤1 to 5 Mt (Herzig and
474 Hannington 1995) with an average size of 2.8 Mt (Barrie and Hannington 1999). They occur at
475 water depths of >1600 m where boiling is prevented by the hydrostatic pressure, and comprise a
476 stockwork zone overlain by zoned massive and semi-massive sulphides (Hannington et al. 1998).
477 The deposits are on average Cu-rich and Pb-Zn-poor compared to other VMS types (e.g. Barrie
478 and Hannington 1999; Table 6). Barrie and Hannington (1999) reported an average mafic VMS
479 composition of 2 % Cu, 1.1 % Zn, 0.1 % Pb and 1.7 ppm Au.

480 The mass balance reported above indicates that significant amounts of Au, As, Sb, Se, S,
481 Cu, Zn and Pb are mobilised from the sheeted dyke and plutonic complexes to the seafloor. Some
482 of these metals are trapped in the mineralisation at the transitional zone or in the upper sheeted
483 dyke section but the majority were most likely transported towards the seafloor. The quantity of
484 metal mobilised from the oceanic crust at ODP 1256D is compared with two different modern-
485 day seafloor VMS systems: the TAG active mound from the Mid-Atlantic Ridge (MAR) and the
486 axial graben VMS deposits at 12°50'N on the East Pacific Rise (EPR). The TAG active mound is
487 probably the most extensively investigated modern-day seafloor VMS deposit and is
488 characteristic of a slow-spreading ridge system (e.g., Humphris et al. 1995; Teagle et al. 1998).
489 The axial graben VMS deposits at 12°50'N EPR are a less extensively investigated VMS system
490 but are characteristic of a fast-spreading ridge system (e.g. Hekinian and Fouquet 1985) which is
491 relevant to the tectonic settings of OPD Hole 1256D.

492 The main ore zone from the 3.8 Mt TAG active mound contains 42.1 % S as sulphide
493 (Hannington et al. 1998) and hosts approximately 1.9 t Au, 16.3 t As, 7.6 t Sb, 53.2 t Se, 79.8 Kt

494 Cu, 22.8 Kt Zn and 274 t Pb (Table 6). To form a hypothetical VMS deposit of similar size and
495 composition from the metals mobilised in the Hole 1256D crust, the sizes of reaction zones
496 required to supply the Au, As, Sb, Se, Cu, Zn and Pb would be 3.3 km^3, 2.4 km^3, 4.1 km^3, 0.4
497 km^3, 3.0 km^3, 0.9 km^3 and 0.6 km^3 respectively (Fig. 10). Sulphide minerals at the TAG active
498 mound have a $^{34}S/^{32}S$ ratio of 6-8 ‰ implying that part of the precipitated S is from hydrothermal
499 fluid dominated by MORB S and the other is from reduced seawater sulphate (Gemmell and
500 Sharpe 1998). Assuming that two thirds of the S has a MORB origin, the reaction zone required
501 to supply the S to the TAG active mound would be 2.4 km^3. These source area size calculations
502 are based on the assumptions that 1) there was no major magmatic input of metals in the
503 hydrothermal fluids, and 2) all of the metals mobilised at depth were transported to the site of
504 deposition. The TAG hydrothermal field formed from many episodes of focused hydrothermal
505 activity over a long period of time (e.g. 20 000 years, Peterson et al. 2000) fed by deep faults in a
506 slow-spreading environment (e.g. McCaig et al., 2007). In contrast, the intense magmatic activity
507 at fast-spreading ridges generally prevents long-lived hydrothermal activity, resulting in the
508 formation of numerous but low tonnage VMS deposits (<3000 t, Hannington et al. 2011).

509 At the East Pacific Rise (EPR) near 12°50'N, Hekinian and Fouquet (1985) reported the
510 presence of 80 small VMS deposits within the ridge axial graben occurring as conical shaped
511 edifices averaging 20 000 tons (Table 6) and characteristic of fast-spreading ridge VMS deposits.
512 Assuming hypothetical axial graben VMS deposits similar to the ones occurring at 12°50'N EPR
513 (0.02 Mt at 34.3 % S, Table 6), the source areas required to mobilise metals from the oceanic
514 crust at Hole 1256D would, for Au, As, Se, Cu, Zn and Pb, be 0.002 km^3, 0.028 km^3, 0.006 km^3,
515 0.017 km^3, 0.002 km^3 and 0.008 km^3, respectively (Fig. 10). Assuming a similar behaviour for S
516 as in the TAG active mound, the reaction zone for S would be 0.016 km^3. These reaction zones

517 are two to three orders of magnitude smaller than the ones required to form a TAG-style deposit,
518 indicating that a relatively small volume of source rock is required to mobilise sufficient metals
519 to form fast-spreading ridge VMS deposits. These differences in element behaviour during VMS
520 formation suggest that although source rock composition controls the hydrothermal fluid
521 composition and thus the type of VMS deposit generated (i.e. alteration of MORB form mafic
522 type VMS; e.g. Franklin et al. 1981), the processes that affect the fraction of metals available for
523 VMS formation, such as metal loss during transport, focus discharge, precipitation efficiency and
524 zone refining, exert key control on the actual bulk metal composition of the VMS deposit.

525 The sizes of the reaction zones required to form VMS deposits are most likely highly
526 variable as they are dependent on multiple parameters including the depth, shape and temperature
527 of the magmatic heat source (Morton and Sleep 1985; Barrie and Hannington 1999; Teagle et al.
528 2003), the porosity of the crust (Barrie and Hannington 1999), the geometry of the circulation cell
529 (e.g. Johnson et al. 2010) and the presence of major faults (McCaig et al. 2007). Ohmoto (1996)
530 estimated a hydrothermal cell size of 40 km^3 to generate Kuroko-type VMS deposits but these
531 deposits form in an arc environment where hydrothermal fluid circulation is most likely enhanced
532 by abundant shallow level intrusions. Using seismic survey data, Tolstoy et al. (2008) identified
533 hydrothermal circulation cell size of ~5 km^3 at near 9°50'N on the fast spreading EPR (500 m
534 width, 1 km depth and ~10 km length along the ridge axis). A 5 km^3 reaction cell in the Hole
535 1256D crust (3.9 km^3 of sheeted dyke complex and 1.1 km^3 of plutonic complex) would mobilise
536 a total of 2.9 t Au, 339 t As, 9 t Sb, 741 t Se, 1.45 Mt S, 0.13 Mt Cu, 0.11 Mt Zn and 2270 t Pb
537 (Table 5).

538 The quantity of metals mobilised from a 5 km^3 reaction cell in Hole 1256D would be
539 enough to form at least ~180 axial graben VMS deposits similar to the ones occurring at 12°50'N

EPR. However, only a small proportion of the mobilised metals are trapped as VMS deposits. The metal budget from the source area to the deposit can be affected by many different processes. For example, metal loss can occur either during migration of hydrothermal fluids from the source areas toward the seafloor (e.g. Hannington 2013), by unfocused discharge of the hydrothermal fluids on the seafloor, by inefficient metal trapping mechanisms during precipitation or by extensive zone refining of VMS deposits (e.g. Petersen et al. 2000). The addition of metals to the hydrothermal fluids can also occur, such as by addition of metal-rich magmatic fluids (e.g. Stanton 1990, Ohmoto 1996). Calculation of the percentages of trapped metal required to form the TAG active mound and the axial graben VMS deposits at 12°50'N EPR from a 5 km^3 reaction cell, as well as the percentage of lost metals, are shown in Figure 11. Significant differences in trapping efficiencies for the different metals in both tectonic settings can be observed (over one order of magnitude maximum). Although Cu and Zn are mobilised in similar quantities from the lower crust (-9.6 % and -7.8 % respectively, Table 5), it appears that Cu is preferentially trapped during VMS formation probably due to higher precipitation efficiency or to preferential fractionation during zone refining. This suggests that precipitation efficiency and/or zone refining might have an important effect on the Cu-rich affinity of the mafic type VMS.

There is a striking difference in metal trapping mechanism efficiencies during VMS formation between the TAG active mound and the axial graben VMS deposits at 12°50'N EPR. In the latter, which are representative of fast-spreading ridges, the trapping efficiencies are less than 1 %, suggesting that of the significant quantity of metals mobilised, only a small portion is trapped as small VMS deposits with the majority being lost. In the TAG active mound the trapping efficiencies from Figure 11 are relatively high (from 7 % to 82 %). However, the greater longevity of slow-spreading ridge hydrothermal cell systems (e.g. 20 000 years; Petersen et al.

563 2000) most likely indicates more extensive and efficient metal mobilisation from the deeper
564 crust. The trapping efficiencies estimated for the TAG active mound are therefore likely to be an
565 overestimate.

566 During VMS formation mobilised metals that are not trapped as VMS mineralisation are
567 vented into seawater. Vented metals can either form particles in plume and sediment as ochres,
568 umbers and metalliferous sediments, or dissolve in seawater (e.g. James and Elderfield 1996). No
569 VMS deposit or fossil hydrothermal vent has been observed in the vicinity of Hole 1256D,
570 although some seamounts are present in the vicinity (Teagle et al. 2006). This suggests that the
571 metals were likely either to be trapped in some form of deposit hidden under the blanketing
572 sediment, or lost by diffuse unfocussed discharge. The main implication for VMS formation from
573 the calculation of the metals mobilised from the oceanic crust at ODP Hole 1256D is that the
574 mobilisation of large masses of metals from alteration zones at deeper levels in the oceanic crust
575 does not always lead to the formation of a VMS deposit, and that metal trapping processes are
576 perhaps more important parameters in the formation of VMS deposit.

577 Implications for Au-rich VMS formation

578 Gold-rich VMS deposits can be defined by either a Au grade >3.46 ppm and a Au
579 tonnage ≥31 t (Mercier-Langevin et al. 2011) or by a Au to base metals ratio over unity (Au in
580 ppm and base metals in per cent; e.g. Poulsen and Hannington 1996). Assuming a 5 km^3 reaction
581 zone, the quantity of Au mobilised from the oceanic crust at ODP Hole 1256D is 2.9 t, which is
582 over an order of magnitude less than that required to form a Au-rich VMS deposit (≥31 t Au).
583 The Au grade of mafic-VMS deposits is also lower than that observed in Au-rich VMS deposits
584 by around an order of magnitude (Table 6), although small deposits such as those in the axial
585 graben at 12°50'N EPR could have the Au grades of Au-rich deposits if the trapping mechanisms

586 for Au increased in efficiency from 0.034 % to 2.40 %. The Au to base metals ratio of the metals
587 mobilised at ODP Hole 1256D (0.12) is similar to that of the TAG active mound (0.21,
588 Hannington et al. 1998) and in the same order of magnitude as average mafic VMS deposits
589 (0.53, Barrie and Hannington 1999). The ratio is one order of magnitude higher than the axial
590 graben VMS deposits at 12°50'N EPR (0.02, Hekinian and Fouquet 1985; Fouquet et al.1988),
591 possibly due to the low trapping efficiency of Au during VMS formation as suggested in Figure
592 11. Whichever classification for Au-rich VMS deposits is used, it appears that Au needs to be
593 enriched by one order of magnitude relative to the other elements for formation of a Au-rich
594 VMS deposit. More effective leaching of Au from the source area, more efficient trapping
595 mechanisms or magmatic input of Au would be required to form a Au-rich VMS deposit from the
596 ODP Hole 1256D crust. The settings where abundant Au-rich VMS deposits occur are
597 characterised by Au-rich source rock (e.g. back-arc basins; Moss et al. 2001; Pitcairn 2011), by
598 abundant shallow level magmatic intrusions that may provide Au-rich magmatic volatiles (e.g.
599 Stanton 1990, Ohmoto 1996), by shallow seawater which allows sub-seafloor boiling and
600 enrichment of Au into a volatile phase (Urabe et al. 1987; Butterfield et al. 1990), or by a
601 combination of the above. Mafic VMS deposits associated with mid-oceanic spreading ridges are
602 unlikely to be Au-rich due to the low Au content of source rocks and the water depth which
603 inhibits sub-seafloor boiling (Herzig and Hannington 1995).

604 ## Conclusions

605 Hydrothermal fluid circulation has a profound effect on the bulk chemistry of the oceanic
606 crust and can lead to the formation of VMS deposits. Analyses, using low detection limit
607 methods, of deep oceanic crust material from ODP Hole 1256D enable us to quantify the

608 mobility of Au, As, Sb, Se ,Te along with S, Cu, Zn and Pb in the oceanic crust. This process is
609 summarised in Figure 12. The major outcomes of this study are:

610 • Gold, Pb, As and Se are efficiently mobilised from the sheeted dyke complex and the
611 plutonic complex by the hydrothermal fluid circulation (-46 %, -44.1 %, -27.2 % and -
612 26.7 %, depletions respectively) followed by Cu, S, Zn and Sb (-9.6 %, -8.4 %, -7.9 %
613 and -2.5 %, depletions respectively). Te appears to be less strongly affected by
614 hydrothermal fluid circulation. The investigated elements, with the exception of Zn, show
615 similar depletion patterns being removed from ~1100-1150 mbsf and downward. Zinc is
616 enriched in the upper sheeted dyke section and is mobilised from ~1300 mbsf. Lead
617 shows enrichment in the upper sheeted dykes similar to Zn.
618 • All elements except Cu are strongly enriched in the sulphide-rich samples of the
619 transitional zone. Arsenic, Sb, Se and Pb are also enriched in background altered basalts
620 from the transition zone, suggesting possible enrichment in silicate or oxide phases. Cu is
621 enriched locally in sulphide-rich samples from the upper sheeted dykes.
622 • Arsenic and Sb are taken up by the volcanic section in background-altered samples during
623 seawater-derived fluid circulation (30.4 % and 24.5 %, respectively). Such enrichments
624 can have implications for mantle wedge contamination during later subduction. In oceanic
625 crust more open to seawater circulation, substantial As and Sb enrichment in the volcanic
626 section could take place and have more impact on mantle wedge contamination.
627 • Precipitation of the mobilised metals during fluid migration from the lower crust towards
628 the seafloor occurs in the upper sheeted dykes (Zn and Pb) and in the transitional zone.
629 The total mass of metals precipitated is, however, a minor proportion to those produced at

630 depth, and the vast majority of mobilised metals are therefore transported towards the
631 seafloor.

632 • Quantity and ratios of metals mobilised from the sheeted dyke and plutonic complexes at
633 ODP Hole 1256D are similar to mafic type VMS deposits. Source areas and percentage of
634 trapped metals are estimated for the formation of the TAG active mound and the axial
635 graben VMS deposits at 12°50'N on the EPR. It is suggested that in fast-spreading ridge
636 systems metal trapping mechanisms are low (≤1 %) during VMS formation, and that only
637 a portion of the quantity of metals mobilised from the oceanic crust is trapped as VMS
638 deposit. This emphasises that important metal mobilisation does not necessarily lead to
639 VMS formation and that trapping processes such as focus flow, precipitation efficiency
640 and zone refining are the key processes for VMS formation.

641 • The Cu-affinity of mafic VMS deposits could be enhanced by two processes: preferential
642 precipitation of Zn, and possibly Pb, in the upper sheeted dykes relative to Cu during
643 hydrothermal fluid migration towards the seafloor, and better trapping mechanisms for Cu
644 relative to Zn and Pb during VMS formation.

645 • The mass of Au mobilised and the Au to base metals ratio of the metals mobilised from
646 the oceanic crust at ODP 1256D are not sufficient to form Au-rich VMS deposits. Both
647 the quantity of Au and an enrichment of Au relative to base metals would have to increase
648 tenfold in order to form Au-rich VMS deposits. This could be achieved through more
649 efficient metal mobilisation from the crust, higher source rock Au content, sub-seafloor
650 boiling causing higher precipitation efficiency, zone refining or by magmatic input in the
651 hydrothermal fluids.

Acknowledgments

This work was funded by Stockholm University and by the Swedish Research Council (PRG 621-2007-4539). The authors would like to thank Ahmad Boskabadi and Adam Engström for the help provided during Au and related elements analyses. Michelle Harris was supported by a NERC PhD studentship and major and trace element analyses by research grants NER/T/S/2003/00048, NE/E001971/1, NE/H012842/1, and NE/I006311/1 to DAHT. This research used samples provided by the ODP and IODP. The ODP was sponsored by the National Foundation (NSF) and participating countries under management of Joint Oceanographic Institutions (JOI). The IODP was supported by NSF; Japan's Ministry of Education, Culture, Sports, Science, and Technology; the European Consortium for Ocean Research Drilling; the Australia-New Zealand IODP Consortium, and the People's Republic of China, Ministry of Science and Technology.

Appendices

Appendix 1& 2:

See tables Appendix 1 and Appendix 2

Appendix 3: Error propagation

The mass balance calculations for all elements except Te are determined using the elemental analyses from Appendix 1 and the differentiation curves calculated from Jenner and O'Neill (2012) database in Appendix 2. The errors associated with the mass balance calculations are controlled by the heterogeneous distribution of metals in the samples analysed and the error margin on the differentiation curves, and errors need to be propagated. The errors on the

673 elemental analyses are determined from repetitive analyses of the reference materials and
674 correspond to their relative standard deviations in Table 1. Reference material TDB-1 is used for
675 Au and Te, WMS-1 for As, Sb and Se, and BIR-1 for Cu, Zn and Pb. Uncertainties on the
676 differentiation curves calculated from Jenner and O'Neill (2012) database are determined by the
677 root mean square deviation (RMSD; Jowitt et al. 2012):

678 $$RMSD = \sqrt{\Sigma(Mc - Mm)^2/n} \quad [5]$$

679 with Mc the calculated metal concentration, Mm the measured metal concentration and n
680 the number of values used to calculated the differentiation curves. The normalised RMSD gives
681 the error associated with the differentiation curves in per cent:

682 $$NRMSD = RMSD/(Mm_{max} - Mm_{min}) * 100 \quad [6]$$

683 with Mm_{max} the highest measured metal concentration and Mm_{min} the lowest measured
684 metal concentration. The RMSD and the NRMSD are shown in Table 3.

685 Errors are propagated with the following equation:

686 $$\sigma_{Mass\ Balance} = \sqrt{\sigma_{Analyses}{}^2 + \sigma_{Diff.\ curves}{}^2} \quad [7]$$

687 where $\sigma_{Mass\ Balance}$ is the error in per cent of the mass balance for a given element, $\sigma_{Analyses}$
688 is the error on the elemental analyses and corresponds to the relative standard deviation of the
689 preferred reference materials in Table 1 and $\sigma_{Diff.\ curves}$ is the error on the differentiation curves
690 corresponding to the NRMSD in Table 3. Error propagation is calculated differently for Te
691 because no differentiation curves could be determined; in equation [7] the $\sigma_{Diff.\ curves}$ is replaced
692 by $\sigma_{Prim.\ crust}$ which corresponds to the relative standard deviation of the primary crust

693 concentration calculated in Table 2. Propagated mass balance errors are shown in Appendix 3
694 table.

695 ## References

696 Alt JC, Anderson TF, Bonnell L (1989) The geochemistry of sulfur in a 1.3 km section of
697 hydrothermally altered oceanic crust, DSDP Hole 504B. Geochim Cosmochim Acta 53:1011-
698 1023

699 Alt JC (1995) Sulfur isotopic profile through the oceanic crust: Sulfur mobility and seawater-
700 crustal sulfur exchange during hydrothermal alteration. Geology 23:585-588

701 Alt JC, Laverne C, Vanko DA, Tartarotti P, Teagle DA, Bach W, Zuleger E, Erzinger J,
702 Honnorez I, Pezard PA (1996) Hydrothermal alteration of a section of upper oceanic crust in the
703 eastern equatorial Pacific: A synthesis of results from Site 504 (DSDP Legs 69, 70, and 83, and
704 ODP Legs 111, 137, 140, and 148). Proceedings of the Ocean Drilling Program: Scientific
705 Results 148:417-434

706 Alt JC, Laverne C, Coggon RM, Teagle DAH, Banerjee NR, Morgan S, Smith-Duque CE, Harris
707 M, Galli L (2010) Subsurface structure of a submarine hydrothermal system in ocean crust
708 formed at the East Pacific Rise, ODP/IODP Site 1256. Geochem Geophys Geosyst 11

709 Alt JC, Shanks WC (2011) Microbial sulfate reduction and the sulfur budget for a complete
710 section of altered oceanic basalts, IODP Hole 1256D (eastern Pacific). Earth Planet Sci Lett
711 310:73-83

712 Arevalo R, McDonough WF (2010) Chemical variations and regional diversity observed in
713 MORB. Chem Geol 271:70-85

714 Barrie C, Hannington M (1999) Classification of volcanic-associated massive sulfide deposits
715 based on host-rock composition. Rev Econ Geol 8:1-11

716 Beaulieu S (2010) InterRidge global database of active submarine hydrothermal vent fields.
717 Version 2.2 http://www.interridge.org/irvents/ (march 2015)

718 Bédard L, Barnes S-J (2002a) A comparison of the capacity of FA-ICP-MS and FA-INAA. J Rad
719 Nucl Chem 254:319-329

720 Bédard L, Barnes S-J (2002b) A comparison of N-type semi-planar and coaxial INAA detectors
721 for 33 geochemical reference samples. J Rad Nucl Chem 254:485-497

722 Butterfield DA, Massoth GJ, McDuff RE, Lupton JE, Lilley MD (1990) Geochemistry of
723 hydrothermal fluids from Axial Seamount hydrothermal emissions study vent field, Juan de Fuca
724 Ridge: Subseafloor boiling and subsequent fluid-rock interaction. J Geophy Res: Solid Earth
725 95:12895-12921

726 Coggon RM, Teagle DAH, Smith-Duque CE, Alt JC, Cooper MJ (2010) Reconstructing past
727 seawater Mg/Ca and Sr/Ca from mid-ocean ridge flank calcium carbonate veins. Science
728 327:1114-1117

729 Constantin M (2009) Trace element data for gold, iridium and silver in seventy geochemical
730 reference materials. Geostand Geoanal Res 33:115-132

731 Coogan LA, Dosso S (2012) An internally consistent, probabilistic, determination of ridge-axis
732 hydrothermal fluxes from basalt-hosted systems. Earth Planet Sci Lett 323:92-101

733 Doe BR (1994) Zinc, copper, and lead in mid-ocean ridge basalts and the source rock control on
734 Zn/Pb in ocean-ridge hydrothermal deposits. Geochim Cosmochim Acta 58:2215-2223

735 Fitton JG, Saunders AD, Larsen LM, Hardarson BS, Norry MJ (1998). Volcanic rocks from the
736 southeast Greenland margin at 63°N: composition, petrogenesis and mantle sources. Proceedings
737 of the Ocean Drilling Program: Scientific Results 152:331–350

738 Fouquet Y, Auclair G, Cambon P, Etoubleau J (1988) Geological setting and mineralogical and
739 geochemical investigations on sulfide deposits near 13ºN on the East Pacific Rise. Marine Geol
740 84:145-178

741 Fouquet Y, Knott R, Cambon P, Fallick A, Rickard D, Desbruyeres D (1996) Formation of large
742 sulfide mineral deposits along fast spreading ridges. Example from off-axial deposits at 12º43′ N
743 on the East Pacific Rise. Earth Planet Sci Lett 144:147-162

744 Franklin J, Lydon J, Sangster D (1981) Volcanic-associated massive sulfide deposits. Econ Geol
745 75:485-627

746 Galley AG, Hannington M, Jonasson I (2007) Volcanogenic massive sulphide deposits. Mineral
747 deposits of Canada: a synthesis of major deposit-types, district metallogeny, the evolution of
748 geological provinces, and exploration methods. Geol Assoc Can, Mineral Deposits Division,
749 Special Publication 5:141-161

750 Geldmacher J, Höfig T, Hauff F, Hoernle K, Garbe-Schönberg D, Wilson D (2013) Influence of
751 the Galápagos hotspot on the East Pacific Rise during Miocene superfast spreading. Geology
752 41:183-186

753 Gemmell JB, Sharpe R (1998) Detailed sulfur-isotope investigation of the TAG hydrothermal
754 mound and stockwork zone, 26 N, Mid-Atlantic Ridge. Proceedings of the Ocean Drilling
755 Program: Scientific Results 158:71-84

756 Goodfellow WD, Franklin JM (1993) Geology, mineralogy, and chemistry of sediment-hosted
757 clastic massive sulfides in shallow cores, Middle Valley, northern Juan de Fuca Ridge. Econ Geol
758 88:2037-2068

759 Hannington MD, Herzig PM, Alt JC (1990) The distribution of gold in sub-seafloor stockwork
760 mineralization from DSDP hole 504B and the Agrokipia B deposit, Cyprus. Can J Earth Sci
761 27:1409-1417

762 Hannington MD, Galley AG, Herzig PM, Petersen S (1998) 28. Comparison of the TAG mound
763 and stockwork complex with Cyprus-type massive sulfide deposits. Proceedings of the Ocean
764 Drilling Program: Scientific Results 158:389-415

765 Hannington MD, Poulsen KH, Thompson JFH, and Sillitoe RH (1999) Chapter 14. Volcanogenic
766 gold in the massive sulfide environment. Volcanic-associated massive sulfide deposits: processes
767 and examples in modern and ancient settings. Rev Econ Geol 8:319-350.

768 Hannington M, Jamieson J, Monecke T, Petersen S, Beaulieu S (2011) The abundance of seafloor
769 massive sulfide deposits. Geology 39:1155-1158

770 Hannington MD (2013) The role of black smokers in the Cu mass balance of the oceanic crust.
771 Earth Planet Sci Lett 374:215-226

772 Harris M (2011) The accretion of lower oceanic crust. University of Southampton, School of
773 Ocean and Earth Science, Doctoral Thesis, 294p

774 Harris M, Coggon RM, Smith-Duque CE, Cooper MJ, Milton JA, Teagle DAH (2015)
775 Channelling of hydrothermal fluids during the accretion and evolution of the upper oceanic crust:
776 Sr isotope evidence from ODP Hole 1256D. Earth Planet Sci Lett 416:56-66

777 Harvey, PK (1989) Automated X-ray fluorescence in geochemical exploration. In: Ahmedali,
778 S.T., (Eds), X-ray fluorescence analysis in the geological sciences; advances in methodology.
779 Geol Assoc Can 221-258

780 Hattori KH, Guillot S (2003) Volcanic fronts form as a consequence of serpentinite dehydration
781 in the forearc mantle wedge. Geology 31:525-528

782 Hattori K, Takahashi Y, Guillot S, Johanson B (2005) Occurrence of arsenic (V) in forearc
783 mantle serpentinites based on X-ray absorption spectroscopy study. Geochim Cosmochim Acta
784 69:5585-5596

785 Hekinian R, Fouquet Y (1985) Volcanism and metallogenesis of axial and off-axial structures on
786 the East Pacific Rise near 13 degrees N. Econ Geol 80:221-249

787 Herzig PM, Hannington MD (1995) Polymetallic massive sulfides at the modern seafloor: A
788 review. Ore Geol Rev10:95-115

789 Humphris SE, Herzig P, Miller D, Alt J, Becker K, Brown D, Brugmann G, Chiba H, Fouquet Y,
790 Gemmell J (1995). The internal structure of an active sea-floor massive sulfide deposit. Nature
791 377: 713–716

792 Huston DL, Large RR (1989) A chemical model for the concentration of gold in volcanogenic
793 massive sulphide deposits. Ore Geol Rev 4:171-200

794 Huston D (2000) Gold in volcanic-hosted massive sulfide deposits: distribution, genesis, and
795 exploration. In: Gold in, 2000: 401-426

796 James R, Elderfield H (1996) Dissolved and particulate trace metals in hydrothermal plumes at
797 the Mid-Atlantic Ridge. Geophys Res Lett 23:3499-3502

798 Jenner FE, O'Neill HS (2012) Analysis of 60 elements in 616 ocean floor basaltic glasses.
799 Geochem Geophys Geosyst 13

800 Johnson HP, Tivey MA, Bjorklund TA, Salmi MS (2010) Hydrothermal circulation within the
801 Endeavour segment, Juan de Fuca Ridge. Geochem Geophys Geosyst 11

802 Jowitt SM, Jenkin GRT, Coogan LA, Naden J (2012) Quantifying the release of base metals from
803 source rocks for volcanogenic massive sulfide deposits: Effects of protolith composition and
804 alteration mineralogy. J Geochem Explor 118:47-59

805 Keays RR, Scott RB (1976) Precious metals in ocean-ridge basalts; implications for basalts as
806 source rocks for gold mineralization. Econ Geol 71:705-720

807 Koepke J, Christie D, Dziony W, Holtz F, Lattard D, MacLennan J, Park S, Scheibner B,
808 Yamasaki T, Yamazaki S (2008). Petrography of the dike-gabbro transition at IODP Site 1256
809 (equatorial Pacific): The evolution of the granoblastic dikes. Geochem Geophys Geosyst 9

810 Korobeynikov AF, Pertsev NN (1995) Distribution of Au and Pd in basalts and diabases in Hole
811 504B, Leg 69 and Leg 140. Proceedings of the Ocean Drilling Program: Scientific Results
812 137/140:117-120

813 Korobeynikov AF, Pertsev NN (1996) Data report: gold content in upper crustal rocks from Hole
814 504B. Proceedings of the Ocean Drilling Program: Scientific Results 148:453-454

815 Leaver ME, Salley J (1994) Certificate of analysis TDB-1. Canadian Certified Reference
816 Materials Project. Natural Resources Canada (Ottawa, Canada).

817 Leaver ME, Salley J (2007) Certificate of analysis WMS-1a. Canadian Certified Reference
818 Materials Project. Natural Resources Canada (Ottawa, Canada).

819 Leaver ME, Salley J (2010) Certificate of analysis CH-4. Canadian Certified Reference Materials
820 Project. Natural Resources Canada (Ottawa, Canada).

821 McCaig AM, Cliff RA, Escartin J, Fallick AE, MacLeod CJ (2007) Oceanic detachment faults
822 focus very large volumes of black smoker fluids. Geology 35:935-938

823 Mercier-Langevin P, Hannington MD, Dube B, Becu V (2011) The gold content of volcanogenic
824 massive sulfide deposits. Miner Deposita 46:509-539

825 Morton JL, Sleep NH (1985) A mid-ocean ridge thermal model: Constraints on the volume of
826 axial hydrothermal heat flux. J Geophy Res: Solid Earth 90:11345-11353

827 Moss R, Scott SD, Binns RA (2001) Gold content of eastern manus basin volcanic rocks:
828 implications for enrichment in associated hydrothermal precipitates. Econ Geol 96:91-107

829 Mudd GM, Weng Z, Jowitt SM (2013) A detailed assessment of global Cu resource trends and
830 endowments. Econ Geol 108:1163-1183

831 Nesbitt HW (1979) Mobility and fractionation of rare earth elements during weathering of a
832 granodiorite. Nature 279:206-210

833 Nesbitt BE, St. Louis RM, Muehlenbachs K (1987) Distribution of gold in altered basalts of
834 DSDP hole 504B. Can J Earth Sci 24:201-209

835 Ohmoto H (1996) Formation of volcanogenic massive sulfide deposits: the Kuroko perspective.
836 Ore Geol Rev10:135-177

837 Patten C, Barnes S-J, Mathez EA, Jenner FE (2013) Partition coefficients of chalcophile elements
838 between sulfide and silicate melts and the early crystallization history of sulfide liquid: LA-ICP-
839 MS analysis of MORB sulfide droplets. Chem Geol 358:170-188

840 Pearce JA, Cann J (1973) Tectonic setting of basic volcanic rocks determined using trace element
841 analyses. Earth Planet Sci Lett 19:290-300

842 Perfit MR, Ridley WI, Jonasson I (1999) Geologic, petrologic and geochemical relationships
843 between magmatism and massive sulfide mineralization along the eastern Galapagos Spreading
844 Center. Rev Econ Geol 8:75-100

845 Petersen S, Herzig P, Hannington MD (2000) Third dimension of a presently forming VMS
846 deposit: TAG hydrothermal mound, Mid-Atlantic Ridge, 26 N. Miner Deposita 35:233-259

847 Pitcairn IK, Warwick PE, Milton JA, Teagle DAH (2006a) Method for ultra-low-level analysis of
848 gold in rocks. Anal Chem 78:1290-1295

849 Pitcairn IK, Teagle DA, Craw D, Olivo GR, Kerrich R, Brewer TS (2006b) Sources of metals and
850 fluids in orogenic gold deposits: insights from the Otago and Alpine Schists, New Zealand. Econ
851 Geol 101:1525-1546

852 Pitcairn IK (2011) Background concentrations of gold in different rock types. Appl Earth Sci
853 120:31-38

854 Poulsen K, Hannington M (1996) Volcanic-associated massive sulphide gold Geology of
855 Canadian Mineral Deposit Types, Geological Survey of Canada. Geol Can 8:183-196

856 Richardson C, Cann J, Richards H, Cowan J (1987) Metal-depleted root zones of the Troodos
857 ore-forming hydrothermal systems, Cyprus. Earth Planet Sci Lett 84:243-253

858 Sano T, Sakuyama T, Ingle S, Rodriguez S, Yamasaki T (2011) Petrological relationships among
859 lavas, dikes, and gabbros from Integrated Ocean Drilling Program Hole 1256D: Insight into the
860 magma plumbing system beneath the East Pacific Rise. Geochem Geophys Geosyst 12

861 Schiffman P, Bettison L, Smith B (1987) Mineralogy and geochemistry of epidosites from the
862 Solea graben, Troodos ophiolite, Cyprus. In: Ophiolites: Oceanic Crustal Analogues: Proceedings
863 of the Symposium "Troodos": 673-683

864 Schiffman P, Smith BM (1988) Petrology and oxygen isotope geochemistry of a fossil seawater
865 hydrothermal system within the Solea Graben, northern Troodos ophiolite, Cyprus. J Geophy
866 Res: Solid Earth 93:4612-4624

867 Sillitoe RH, Hannington MD, Thompson JF (1996) High sulfidation deposits in the volcanogenic
868 massive sulfide environment. Econ Geol 91:204-212

869 Stanton R (1990) Magmatic evolution and the ore type-lava type affiliations of volcanic
870 exhalative ores. Australasian Institute of Mining & Metallurgy Proceeding 15:101-107

871 Staudigel H (2003) Hydrothermal alteration processes in the oceanic crust. Treatise on
872 Geochemistry 3:511-535

873 Teagle DA, Alt JC, Chiba H, Humphris SE, Halliday AN (1998) Strontium and oxygen isotopic
874 constraints on fluid mixing, alteration and mineralization in the TAG hydrothermal deposit.
875 Chem Geol 149:1-24

876 Teagle DA, Bickle MJ, Alt JC (2003) Recharge flux to ocean-ridge black smoker systems: a
877 geochemical estimate from ODP Hole 504B. Earth Planet Sci Lett 210:81-89

878 Teagle DAH, Alt, JC, Umino S, Miyashita S, Banerjee NR, Wilson DS (2006) Expedition
879 309/312 Scientists Superfast Spreading Rate Crust 2 and 3. Proceedings of the Ocean Drilling
880 Program 309/ 312: 50

881 Teagle D, Harris M (2011) Drilling gabbro in intact ocean crust formed at a superfast spreading
882 rate. Integrated Ocean Drilling Program Expedition 335 preliminary report: superfast spreading
883 rate crust 4.

884 Tolstoy M, Waldhauser F, Bohnenstiehl D, Weekly R, Kim W-Y (2008) Seismic identification of
885 along-axis hydrothermal flow on the East Pacific Rise. Nature 451:181-184

886 Urabe T, Yuasa M, Nakao S (1987) Hydrothermal sulfides from a submarine caldera in the
887 Shichito-Iwojima Ridge, northwestern Pacific. Marine Geol 74:295-299

888 Violay M, Pezard PA, Ildefonse B, Célérier B, Deleau A (2012) Structure of the hydrothermal
889 root zone of the sheeted dikes in fast-spread oceanic crust: a core-log integration study of ODP
890 Hole 1256D. Eastern Equatorial Pacific Ofioliti 37:1-11

891 Webber AP, Roberts S, Taylor RN, Pitcairn IK (2013) Golden plumes: Substantial gold
892 enrichment of oceanic crust during ridge-plume interaction. Geology 41:87-90

893 Wilson DS, Teagle DAH, Acton GD et al. (2003) Leg 206 summary. Shipboard scientific party.
894 Proceedings of the Ocean Drilling Program: Initial Reports 206

895 Wilson DS et al. (2006) Drilling to gabbro in intact ocean crust. Science 312:1016-1020

Yi W, Halliday AN, Alt JC, Lee D-C, Rehkämper M, Garcia MO, Langmuir CH, Su Y (2000) Cadmium, indium, tin, tellurium, and sulfur in oceanic basalts: Implications for chalcophile element fractionation in the Earth. J Geophys Res: Solid Earth 105:23761-23761

Figure captions

Figure 1: Lithostratigraphy at ODP Hole 1256D with sample locations and Mg#, Y and K_2O as indicators of the degree of differentiation and seawater alteration. Major secondary minerals and temperature are also shown. Modified from Teagle et al. (2006) and Alt et al. (2010).

Figure 2: Concentrations of Au, As, Sb, Se and Te in drill core samples from ODP Hole 1256D. The type of alteration is indicated on the figure. The Hole 1256D median value and MORB average value are also shown. Median MORB value for Au is from Webber et al. (2013), average MORB values for As, Sb and Se are from Arevalo and McDonough (2010) and average MORB value for Te is from Yi et al. (2000).

Figure 3: Box plot of the Au, As, Sb, Se and Te content of all the samples in the four major lithological units in Hole 1256D. The boxes represent 95 % of the data, bars within the box are the medians, dash lines are the average values and external lines are the extreme values.

Figure 4: Concentrations of S, Cu, Zn and Pb in drill core samples from ODP Hole 1256D. The type of alteration is indicated on the figure. The Hole 1256D median value and MORB average value are also shown. Average MORB values are from Arevalo and McDonough (2010).

Figure 5: Au and related element concentrations plotted versus Y concentrations. Light grey crosses correspond to Pacific Ocean MORB fresh glass samples from the Jenner and O'Neill (2012) database, with the exception of Te which represents the Mid-Atlantic Ridge database from (Yi et al. 2000). Light grey differentiation curves are calculated from the Jenner and O'Neill (2012) database whilst the red curves correspond to the Hole 1256D corrected differentiation curves. The style of alteration is indicated on the figure. Plain red squares represent the average composition of least altered samples. Arrows are data plotting outside the axes. See text for calculations.

Figure 6: Sulphur, Cu, Zn and Pb concentrations plotted versus Y concentrations. Light grey crosses correspond to Pacific Ocean MORB fresh glass samples from the Jenner and O'Neill (2012) database. Light grey differentiation curves are those calculated from the Jenner and O'Neill (2012) database whilst the red curves correspond to Hole 1256D corrected differentiation curves. The style of alteration is indicated on the figure. Plain red squares represent the average composition of least altered samples. Arrows are data plotting outside the axes. See text for calculations.

Figure 7: Mass variation of Au and related elements in ODP Hole 1256D drill core samples relative to depth in the section. The type of alteration is indicated on the figure.

Figure 8: Mass variation of S, Cu, Zn and Pb in ODP Hole 1256D drill core samples relative to depth in the section. The type of alteration is indicated on the figure.

Figure 9: Plots of As, Sb, K_2O and Rb in the volcanic section. The type of alteration is indicated on the figure. Dashed equation lines correspond to background altered samples and plain ones to all the samples.

938 Figure 10: Hypothetical reaction zones in Hole 1256D crust from which sufficient metals
939 are mobilised to form a) a deposit of the size and composition of the TAG active mound and b)
940 deposits of the size and composition of the axial graben VMS deposits at 12°50'N EPR. Neither
941 the Sb and Te reaction zones for the axial graben VMS deposits at 12°50'N EPR nor the Te
942 reaction zone for the TAG active mound can be calculated. The graphic representations of the
943 reaction zones are characterised by x=1/2y=z.

944 Figure 11: Mass of metals mobilised from a $5km^3$ reaction zones and the efficiency of
945 metal trapping mechanisms needed to form a) the TAG active mound and b) the axial graben
946 VMS deposits at 12°50'N on the EPR. Percentage of metal lost is also shown along with some of
947 the processes that contribute to metal loss during VMS formation.

948 Figure 12: Interpretation of the behaviour of Au, Au-related elements, S, Cu, Zn and Pb in
949 the oceanic crust during hydrothermal fluid circulation at ODP Hole 1256D. Relative
950 mobilisations of the different elements and hypothetical location of ODP Hole 1256D drill core
951 are indicated.

Figure 1

Click here to download Figure: Fig.1-01.tif

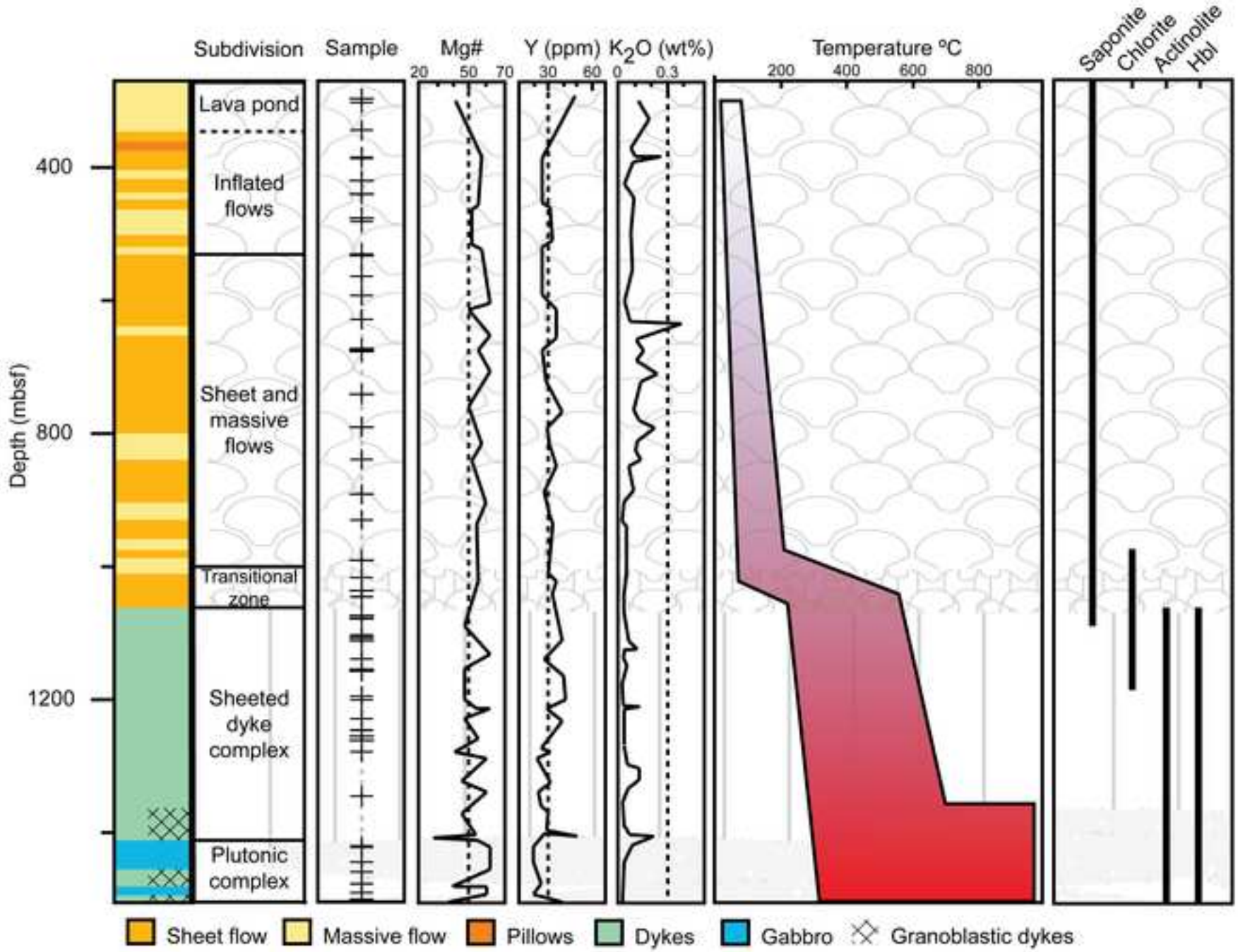

Figure 1

Figure 2

Click here to download Figure: Fig.2-01.tif

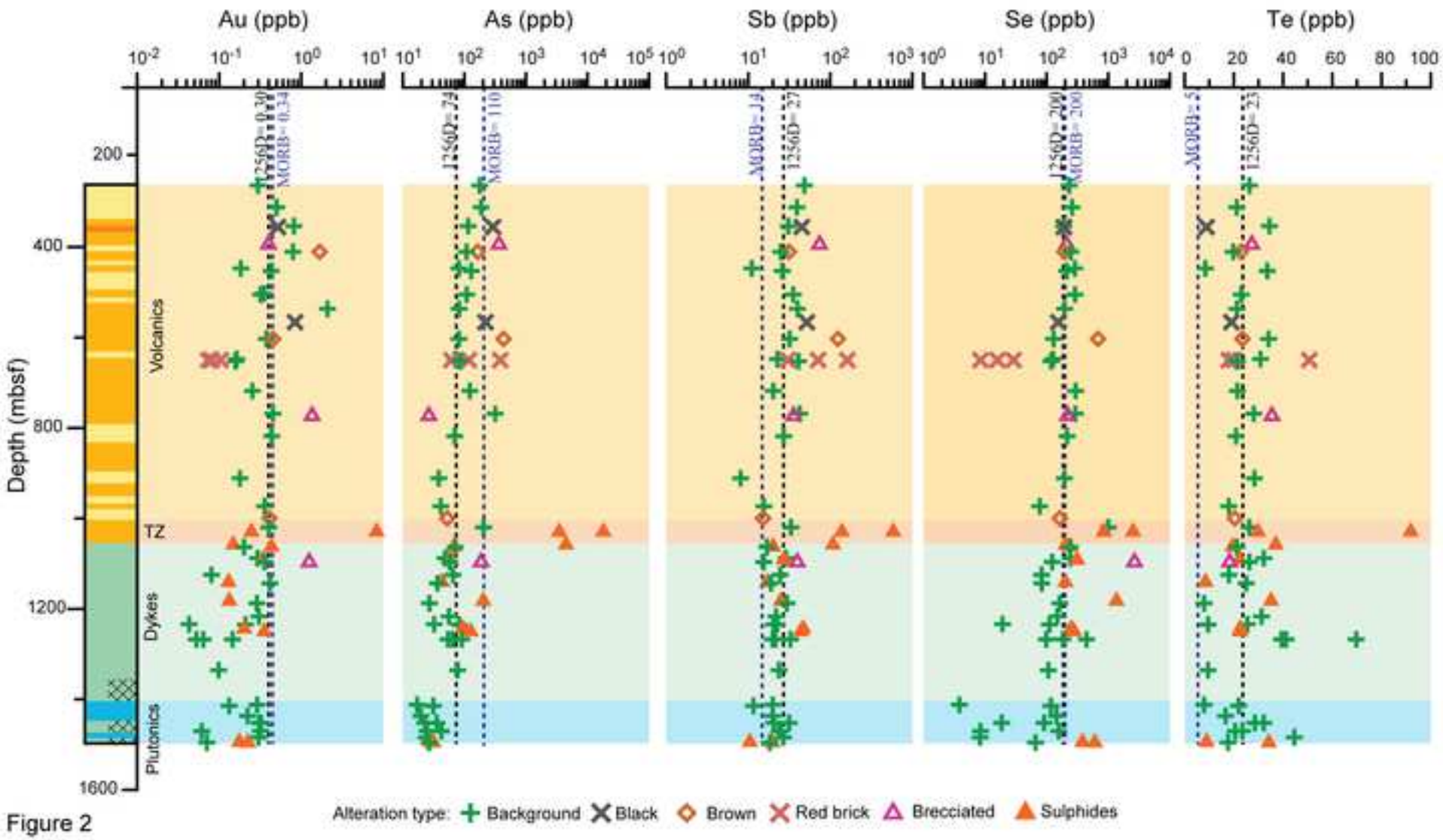

Figure 2

Figure 3

Click here to download Figure: Fig.3-01.tif

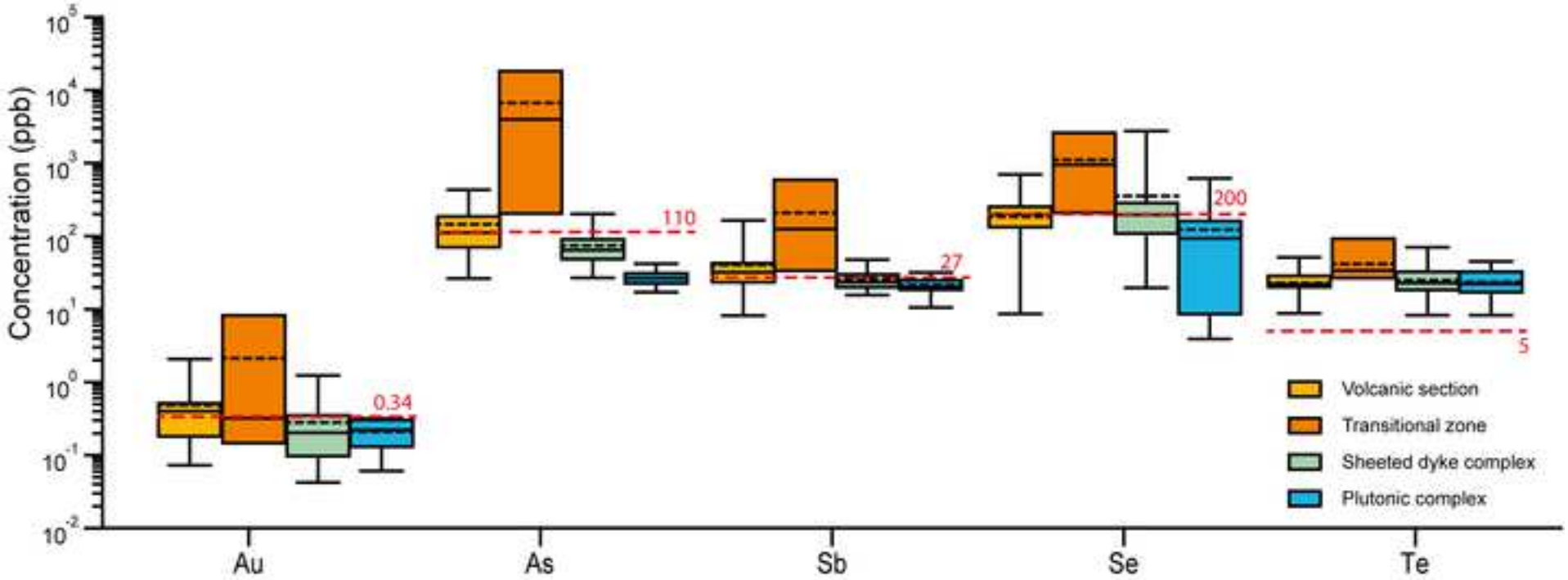

Figure 3

Figure 4

Click here to download Figure: Fig.4-01.tif

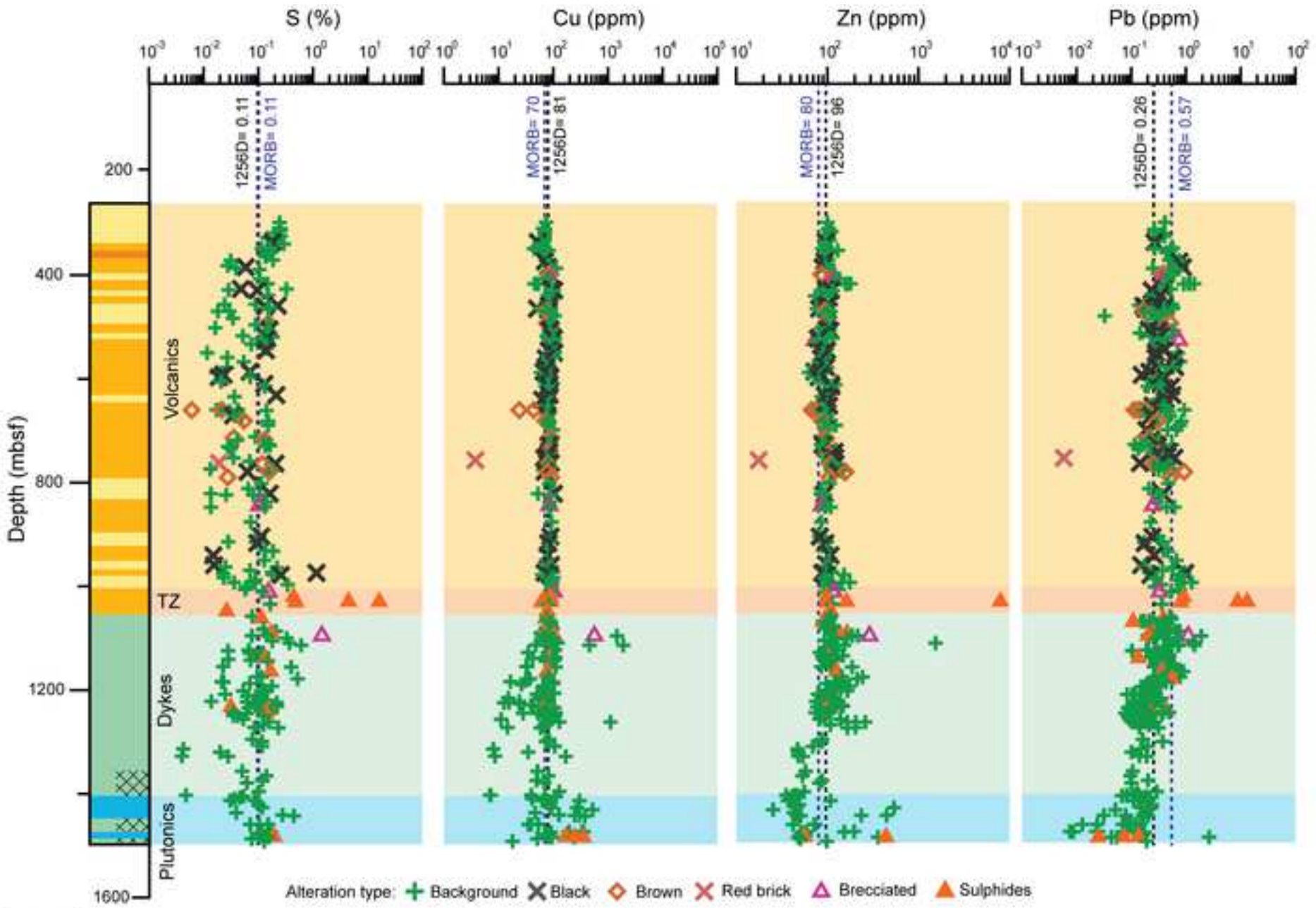

Figure 4

Figure 5
Click here to download Figure: Fig.5-01.tif

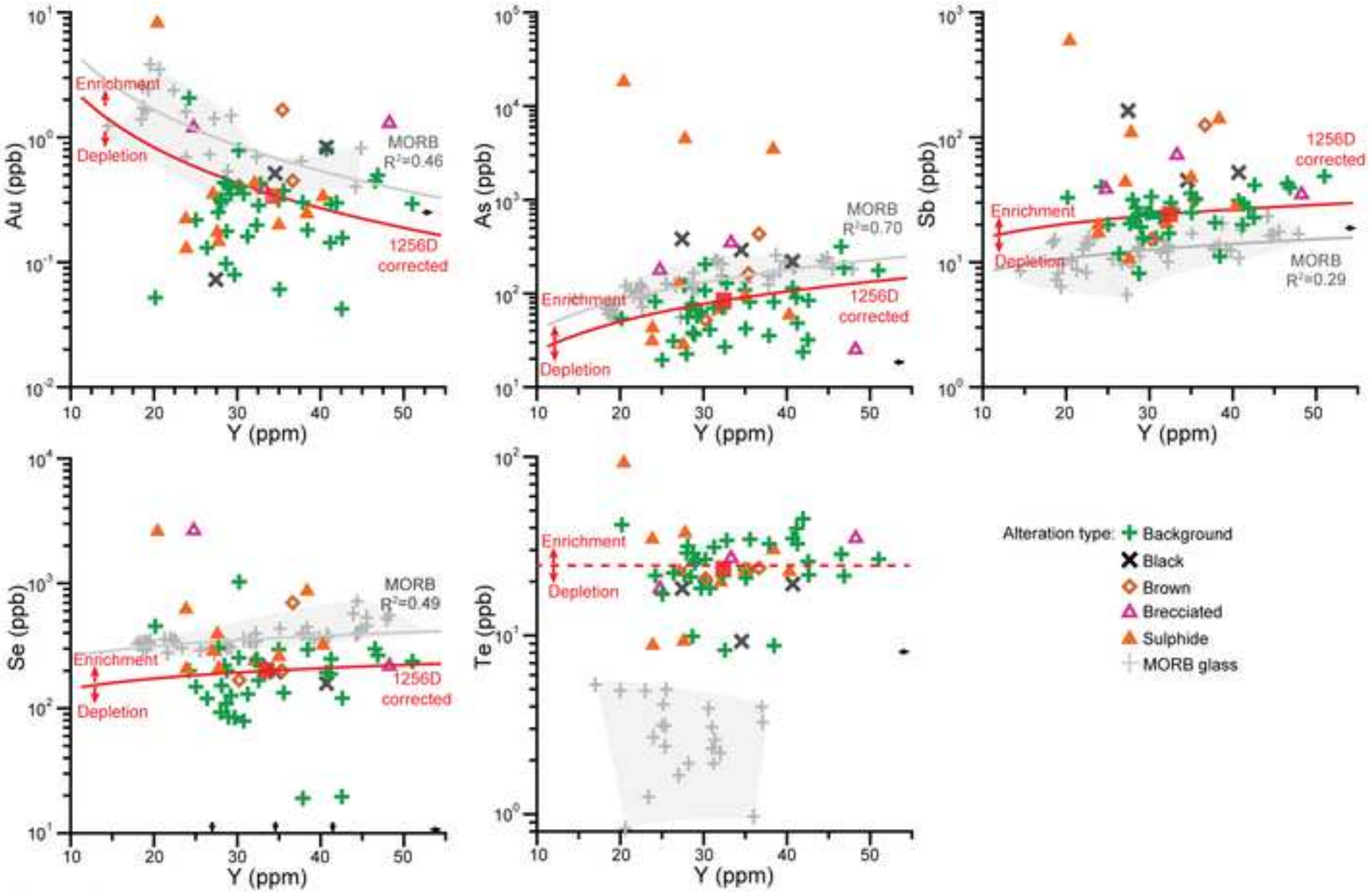

Figure 5

Figure 6
Click here to download Figure: Fig.6-01.tif

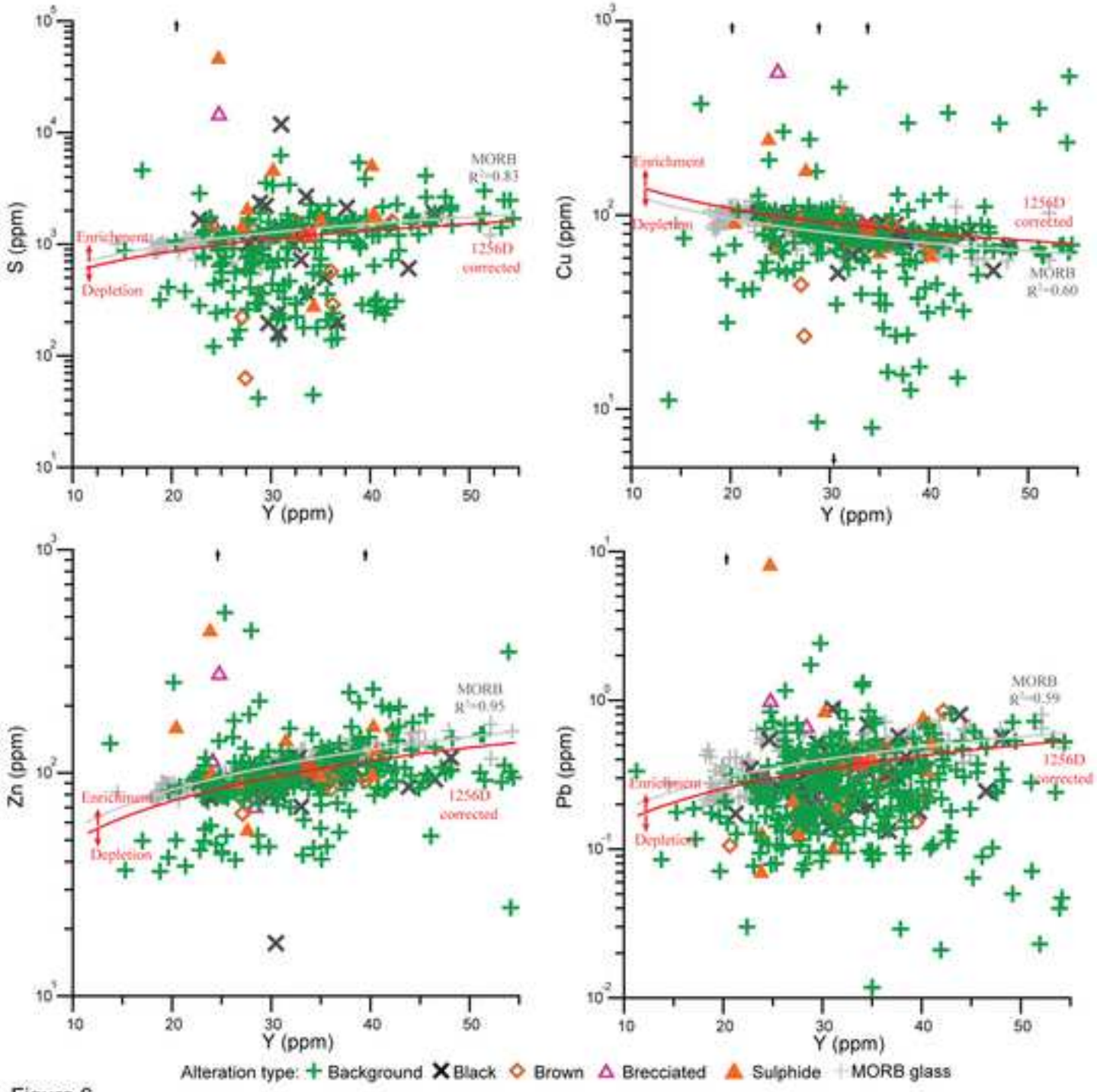

Figure 6

Figure 7
Click here to download Figure: Fig.7-01.tif

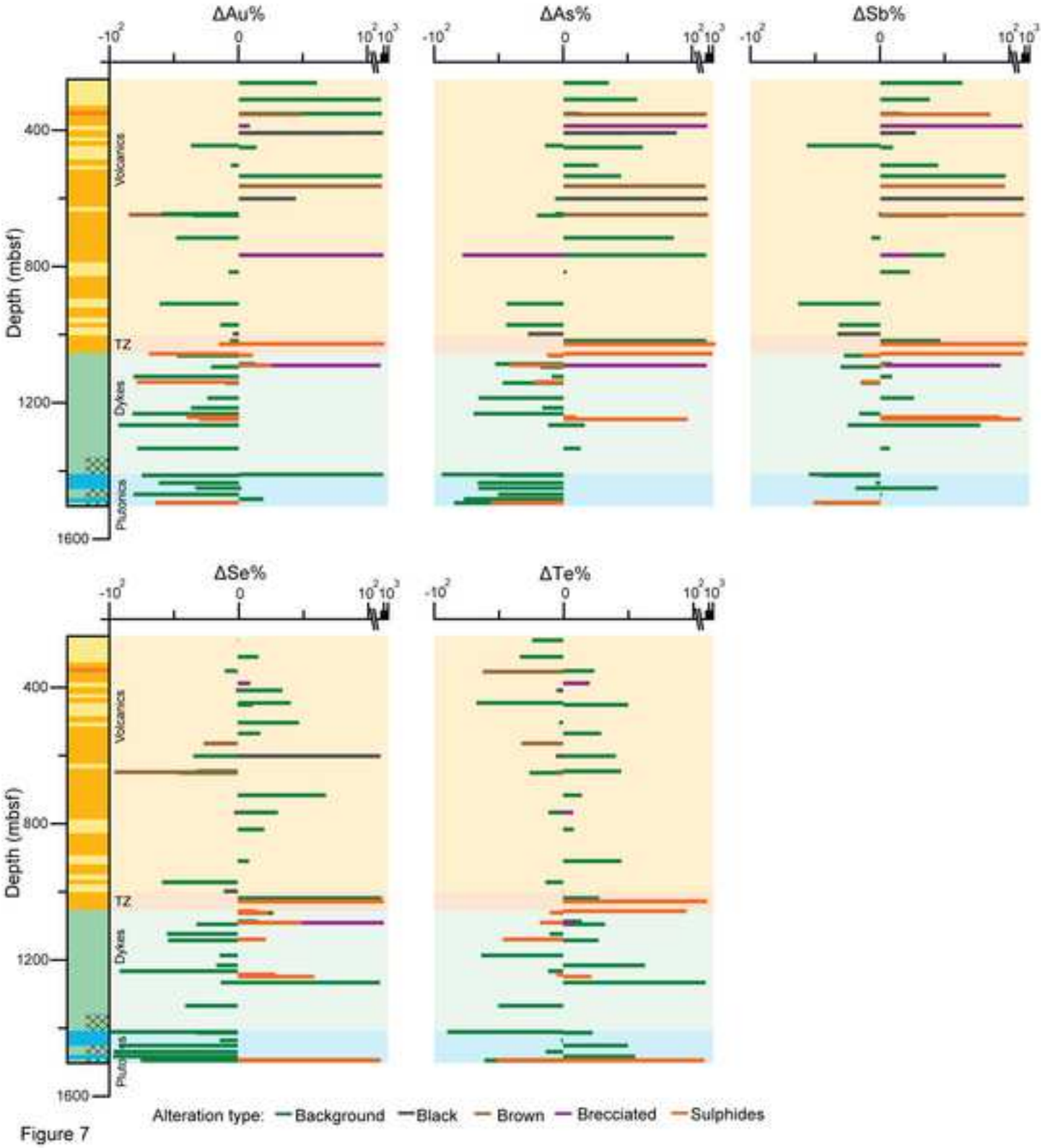

Figure 7

Figure 8
Click here to download Figure: Fig.8-01.tif

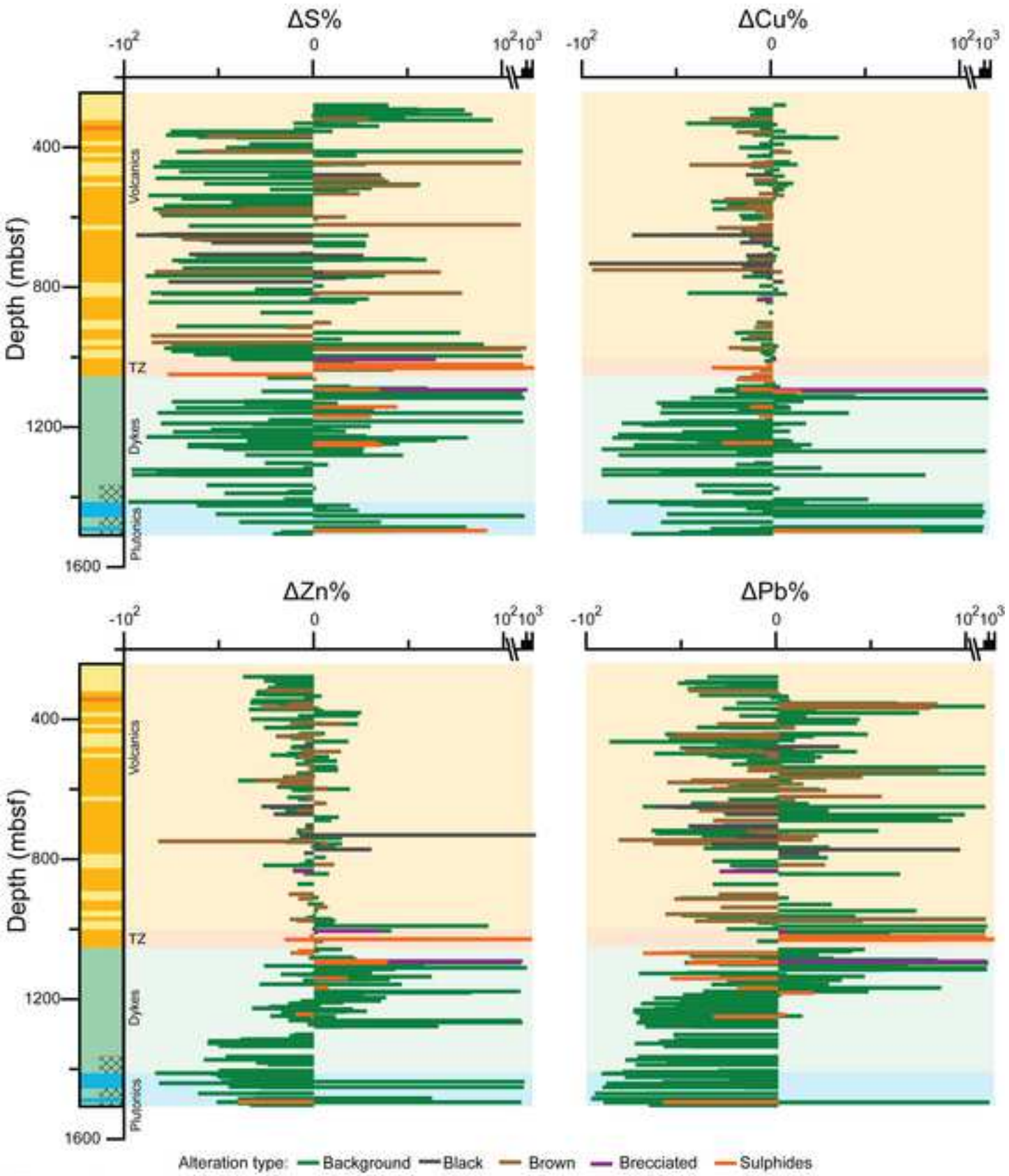

Figure 8

Figure 9
Click here to download Figure: Fig.9-01.tif

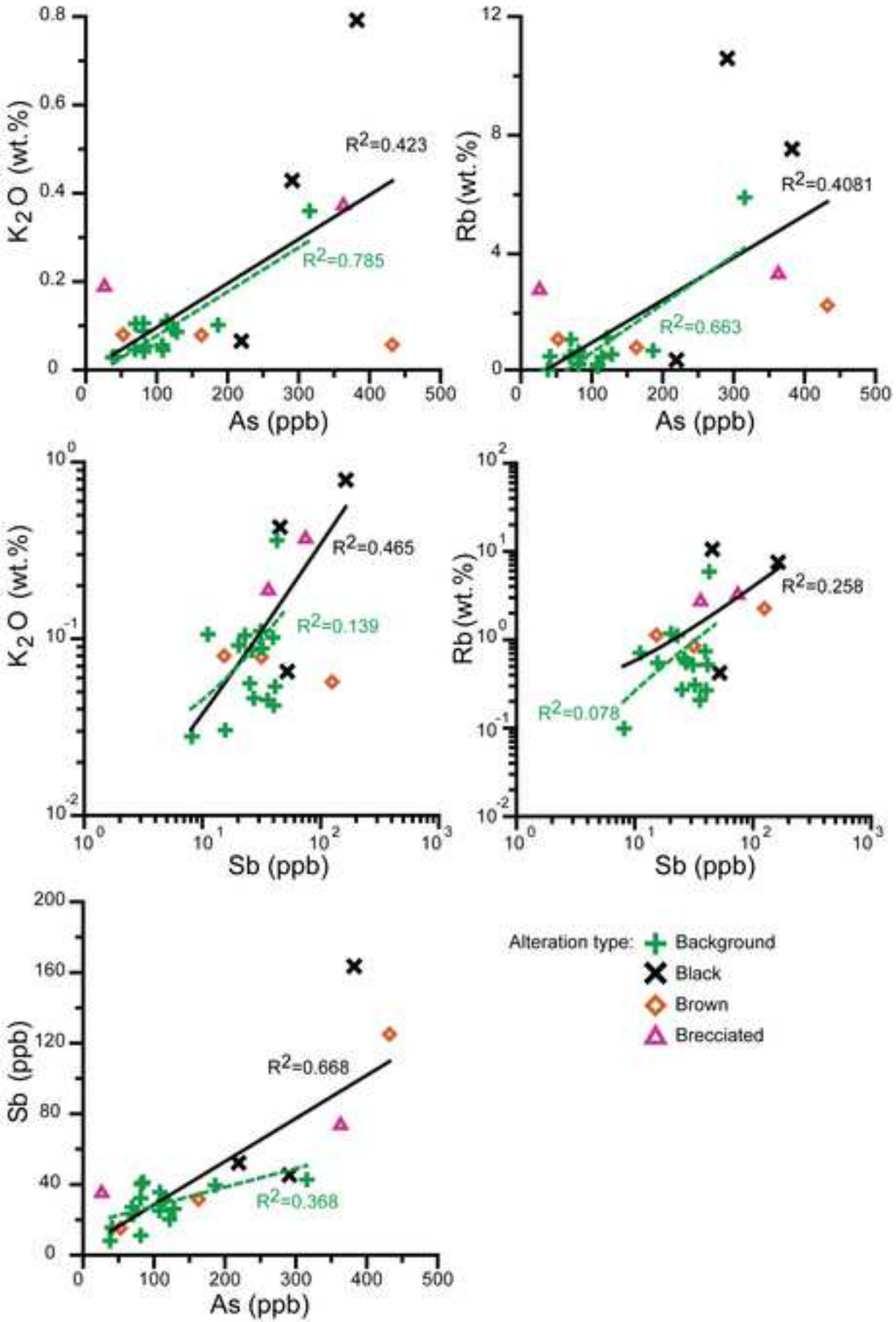

Figure 9

Figure 10
Click here to download Figure: Fig.10-01.tif

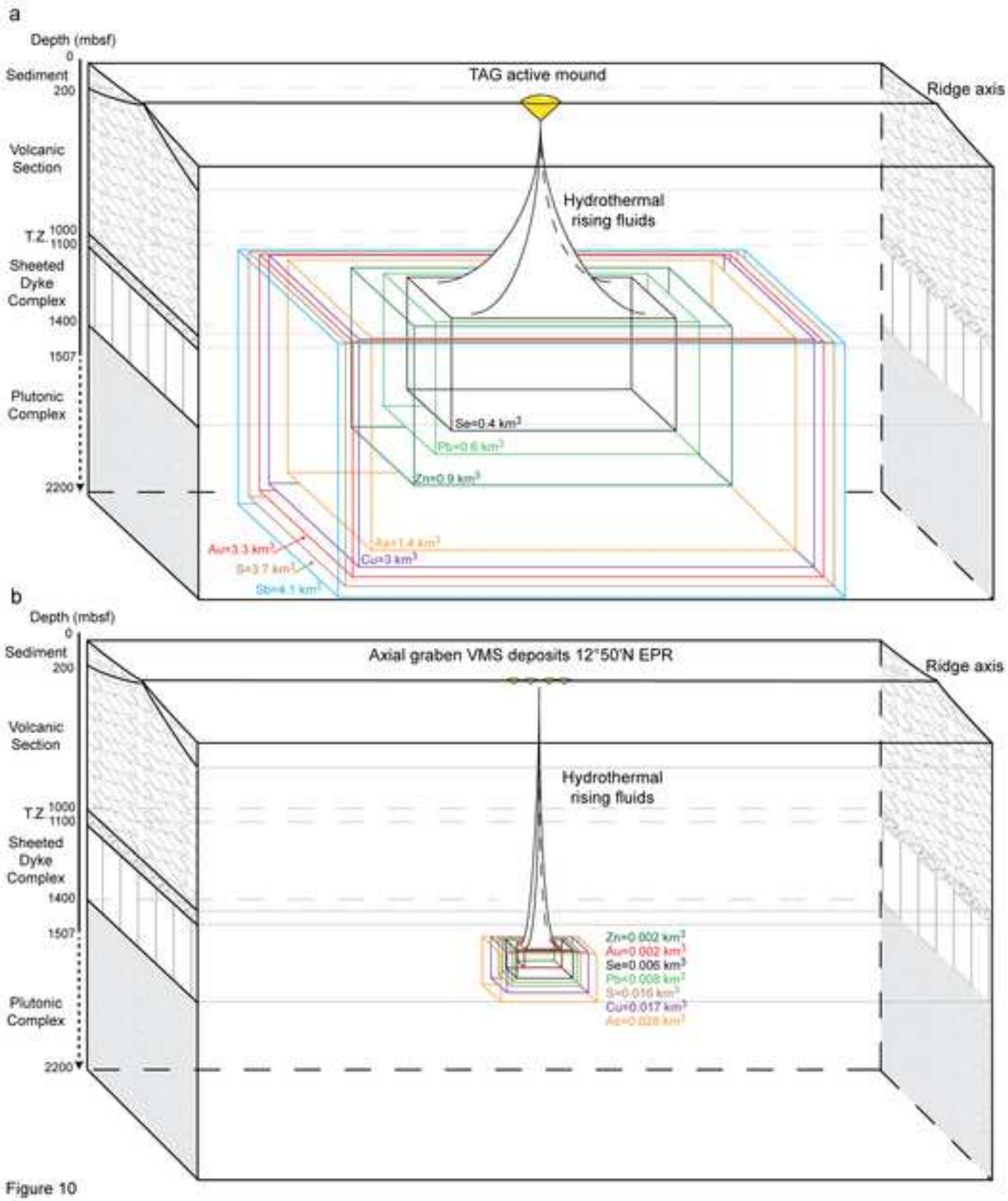

Figure 10

Figure 11

Click here to download Figure: Fig.11-01.tif

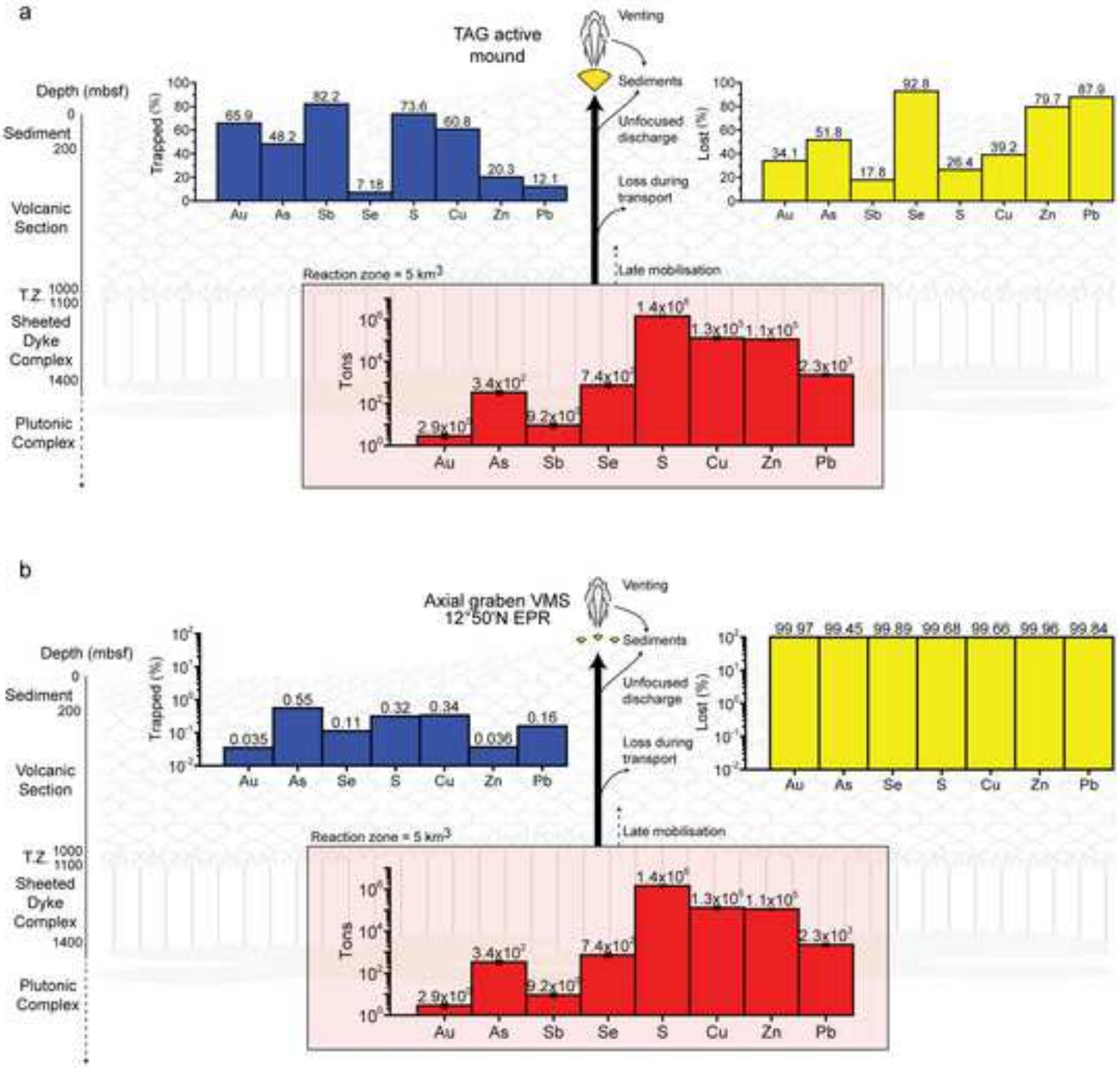

Figure 11

Figure 12

Click here to download Figure: Fig.12-01.tif

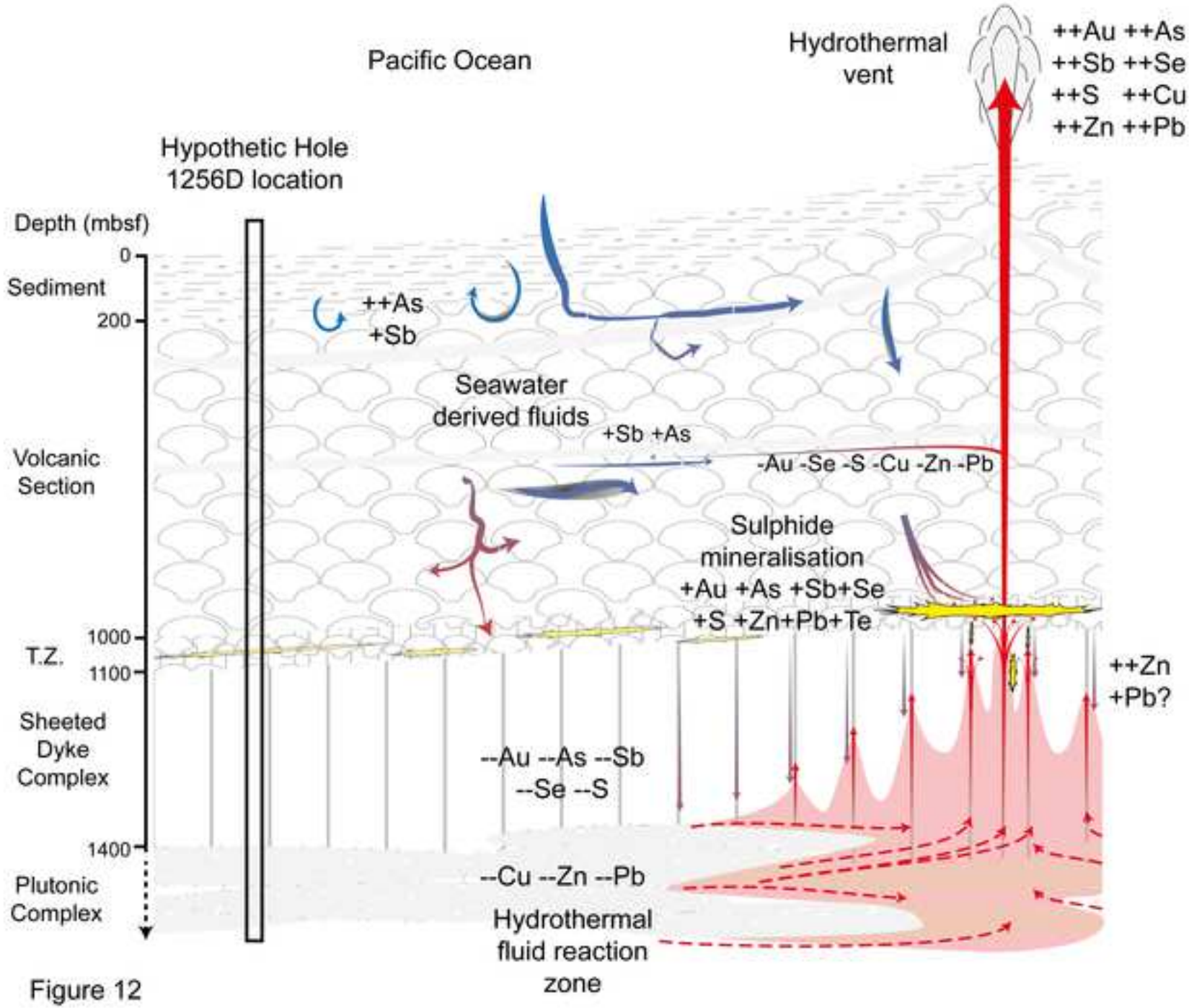

Figure 12

Table 1

Au and related elements

Element	Reference Material	n	Average (ppm)	σ (ppm)	RSD	Published values (ppm)	σ (ppm)	RSD	Recovery rate	References Method	References
Au	TDB-1	9	6.37	0.51	7.9	6.3	1.34	21.3	101.1	ICP-MS	Bédard and Barnes, 2002a
	WMS-1	7	208.9	65.9	31.5	246	44	17.9	84.9	INAA	Constantin, 2009
	CH-4	7	632.3	145.7	23.0	713	62	8.7	88.7	INAA	Constantin, 2009
	BIR-1	5	2.21	0.37	16.7	2.53	0.21	8.3	87.4	INAA	Constantin, 2009
	BAS 206*	6	0.24	0.15	62.5						
As	TDB-1	15	2.08	0.37	17.8	2.2	0.3	13.6	94.5	INAA	Bédard and Barnes, 2002b
	WMS-1	10	23.6	2.83	12.0	19.1	0.7	3.7	123.6	INAA	Bédard and Barnes, 2002b
	CH-4	15	7.57	0.74	9.8	8.8	0.5	5.7	86.0		Leaver and Shalley (2010)**
	BAS 206*	6	450.7	83	18.4						
Sb	TDB-1	16	0.75	0.31	41.3	0.72	0.03	4.2	104.2	INAA	Bédard and Barnes, 2002b
	WMS-1	12	7.21	0.89	12.4	6.92	1	14.5	104.2		Leaver and Shalley (2007)**
	CH-4	9	0.79	0.39	49.4	0.77	0.4	51.9	102.6		Leaver and Shalley (2010)**
	BAS 206*	4	37.9	14.1	37.3						
Se	TDB-1	14	0.41	0.1	24.4	0.7			58.6		Leaver and Shalley (1994)**
	WMS-1	5	75.38	11.68	15.5	87			86.6		Leaver and Shalley (2007)**
	CH-4	12	1.94	0.14	7.2	2.1	0.2	9.5	92.4		Leaver and Shalley (2010)
	BAS 206*	5	256.9	18.3	7.1						
Te	TDB-1	7	0.198	0.04	20.5	0.2			99.0		Leaver and Shalley (1994)**
	WMS-1	7	2.29	0.69	30.1						
	CH-4	7	0.37	0.11	29.7						
	BAS 206*	5	53.5	32.9	61.6						

Sulphur and base metals***

Element	Reference Material	n	Accuracy (%)	Precision (%)	Element	Reference Material	n	Accuracy (%)	Precision (%)
S	BAS ECRM 877-1	60	10.11	5.05	Zn	BIR-1	7	-2.32	0.51
						BHVO-1	7	-0.96	0.48
Cu	BIR-1	7	4.56	0.45		BCR-1	7	-1.32	0.93
	BHVO-1	7	-1.87	0.30					
	BCR-1	7	-0.97	0.53	Pb	BIR-1	7	10.87	3.45
						BHVO-2	7	-0.79	7.57

Table 1. Reference materials and internal standards used for whole rock analyses. *(ppb).**not certified values.*** See Harris (2011) for details

Table 2

Sample	Depth (mbsf)	Y	K2O	S	Zn	Cu	Pb	**Au**	**As**	**Sb**	**Se**	**Te**
		ppm	%	%	ppm	ppm	ppm	**ppb**	**ppb**	**ppb**	**ppb**	**ppb**
1256D 22R-3 13-20	408.7	30.18	0.06	0.34	96.69	90.56	0.48	**0.78**	**107.76**	**25.14**	**253.11**	**20.08**
1256D 27R-1 5-12	445.5	38.45	0.11	0.16	97.84	85.29	0.37	**0.18**	**81.21**	**11.14**	**295.10**	**8.76**
1256D 28R-1 0-8	450.9	32.78	0.09		97.60	83.80	0.22	**0.42**	**128.18**	**26.16**	**217.67**	**33.96**
1256D 35R-2 14-20	490.4	35.41	0.05	0.15	103.2	82.3	0.54					
1256D 37R-3 24-30	503.3	34.97	0.04	0.19	95.01	83.93		**0.32**	**108.49**	**35.64**	**295.91**	**23.37**
1256D 52R-1 65-75	601.4	35.56	0.09		102.90	71.50	0.18	**0.37**	**81.22**	**32.21**	**132.85**	**34.51**
1256D 57R-4 118-125	650.8	42.62	0.05	0.03	91.35	76.24	0.44	**0.16**	**84.47**	**41.28**	**120.55**	**21.78**
1256D 99R2 101-120	909.9	28.74	0.03	0.09	92.56	88.28	0.16	**0.18**	**38.11**	**8.15**	**199.98**	**28.74**
1256D 110R2 76-88	971.9	30.77	0.03	0.02	96.59	77.27	0.22	**0.35**	**41.04**	**15.62**	**78.94**	**18.32**
Glass values from Geldmacher et al. (2013)												
1256D 14R-1 139-142	360.9				100	79.1	0.75					
1256D 17R-1 65-68	374.2				103	89.4	0.35					
1256D 18R-1 81-84	378.8				110	92.3	0.33					
1256D 20R-1 33-37	387.7				117	85.5	0.38					
1256D 21R-1 116-119	398.0				175	48.2	1.07					
1256D 23R-2 16-20	411.9				112	92.8	0.3					
1256D 30R-1 44-59	461.8				95.9	105	0.03					
1256D 38R-1 121-124	505.5				92.4	106	0.36					
1256D 40R-1 31-36	517.8				87.1	104	0.31					
1256D 43R-1 9-12	534.0				91.6	104	0.28					
1256D 51R-2 60-64	598.2				119	79.4	0.43					
1256D 62R-1 10-12	687.3				97.9	98.9	0.42					
Average primary crust composition		**34.39**	**0.06**	**0.12***	**103.55**	**86.85**	**0.38**	**0.35**	**83.81**	**24.42**	**199.26**	**23.69**
σ		**4.36**	**0.03**	**0.2***	**18.42**	**13.43**	**0.22**	**0.20**	**31.81**	**11.91**	**81.81**	**8.59**

Table 2. Average primitive crust compostion calculated from least altered samples. σ = relative standard deviation. * prefered S magmatic value from Alt and Shanks (2011).

Table 3

Element	MORB					Hole 1256D corrected				
	A	B	R^2	RMSD	NRMSD	A	B	R^2	RMSD	NRMSD
Au	210.86	-1.678	0.46	0.84	23.7	105.81	-1.678	0.46	0.84	23.73
As	3.423	1.121	0.70	31.45	15.6	1.590	1.121	0.70	31.45	15.63
Sb	2.1798	0.5102	0.29	3.10	17.4	4.02	0.5102	0.29	3.10	17.36
Se	79.94	0.447	0.49	65.13	14.5	40.99	0.447	0.49	65.13	14.48
S	153.84	0.616	0.83	97.68	6.9	135.66	0.616	0.83	97.68	6.89
Cu	334.8	-0.416	0.60	11.16	16.6	378.3	-0.416	0.60	11.16	16.65
Zn	13.81	0.603	0.95	6.24	6.4	12.28	0.603	0.95	6.24	6.41
Pb	0.0341	0.720	0.59	0.10	13.7	0.0298	0.720	0.59	0.10	13.71

Table 3. Regression coefficients and correlation coefficients used for equation 1. RMSD= root mean square of deviations. RMSD in ppb for Au, As, Sb and Se and in ppm for S, Cu, Zn and Pb. NRMSD= normalised RMSD in perc cent. MORB values are determined from Jenner and O'Neill (2012) database.

Table 4

			Δ Au %	Δ As %	Δ Sb%	Δ Se %	Δ Te %	Δ S %	Δ Cu %	Δ Zn %	Δ Pb %
Volcanic section	Background altered samples	**median**	**3.7**	**20.0**	**19.9**	**13.8**	**2.7**	**-10.5**	**-4.7**	**-4.5**	**-4.6**
		average	37.1	25.3	17.1	7.3	4.8	-12.6	-5.6	-4.0	2.8
		min	-61.7	-44.5	-63.4	-58.4	-66.9	-88.8	-46.0	-39.4	-89.1
		max	239.1	168.2	96.9	68.1	50.3	223.9	34.8	94.7	278.2
		n	16	16	16	16	16	107	140	140	141
	Specific alteration (brown, black and breccia)	**median**	**47.0**	**180.8**	**90.8**	**-2.4**	**-4.0**	**1.7**	**-9.4**	**-5.5**	**-16.3**
		average	150.4	194.9	182.2	14.1	-9.7	20.4	-13.8	797.7	-10.7
		min	-85.4	-78.6	-33.2	-95.2	-61.1	-94.0	-97.5	-82.1	-84.3
		max	571.7	487.3	651.5	241.7	20.7	953.5	9.2	46616.1	153.4
		n	8	8	8	8	8	35	59	59	69
	Median volcanic section	**93.5% bck; 6.5% sp. alt.**	**6.6**	**30.4**	**24.5**	**12.7**	**2.2**	**-9.7**	**-5.0**	**-4.6**	**-5.3**
Transitional zone	Background altered samples	**median**	**-38.4**	**3426.7**	**222.2**	**230.7**	**61.7**	**22.1**	**-6.8**	**6.3**	**45.7**
		average	-38.4	3426.7	222.2	230.7	61.7	13.4	-9.8	8.6	31.3
		min	-70.0	181.5	46.5	15.2	28.0	-24.4	-18.1	3.2	-11.2
		max	-6.8	6672.0	397.9	446.3	95.4	42.4	-4.5	16.4	59.3
		n	2	2	2	2	2	3	3	3	3
	Mineralised samples	**median**	**453.7**	**21170.2**	**1752.1**	**902.2**	**285.0**	**308.2**	**-14.2**	**2.8**	**1380.9**
		average	453.7	21170.2	1752.1	902.2	285.0	4791.8	-17.4	1796.9	1851.5
		min	-15.6	3559.9	443.1	315.7	14.1	-77.2	-32.4	-14.7	79.1
		max	922.9	38780.6	3061.0	1488.6	555.8	18893.3	-3.2	8888.2	4565.1
		n	2	2	2	2	2	6	6	6	5
Sheeted dyke complex	Background altered samples	**median**	**-44.4**	**-16.6**	**0.00**	**-16.6**	**14.6**	**-14.7**	**-10.6**	**1.19**	**-35.3**
		average	-46.4	-24.7	1.2	-7.5	21.8	1.9	22.3	18.6	-21.9
		min	-93.6	-70.0	-30.7	-91.1	-63.2	-96.3	-90.8	-57.8	-80.7
		max	12.8	16.5	77.3	190.1	199.4	455.1	2046.9	1222.5	426.8
		n	11	11	11	11	11	70	124	124	175
	Sulphide-rich	**median**	**-9.99**	**-1.5**	**48.30**	**39.40**	**-7.52**	**35.29**	**-7.43**	**8.94**	**-28.08**
		average	-0.8	41.7	43.9	279.3	-8.0	230.0	44.1	34.9	-1.4
		min	-79.4	-41.3	-15.2	21.8	-46.5	1.8	-26.8	-10.4	-71.5
		max	110.0	220.9	103.3	1492.2	22.0	1426.8	469.1	231.5	241.2
		n	6	6	6	6	6	8	9	9	10
Plutonic complex	All samples	**median**	**-51.7**	**-64.1**	**-11.4**	**-61.9**	**10.6**	**13.1**	**-6.3**	**-39.5**	**-75.7**
		average	6.4	-65.4	-17.7	-16.8	4.7	28.4	75.9	18.4	-54.1
		min	-81.9	-94.6	-55.2	-98.8	-89.3	-98.0	-87.7	-83.7	-98.8
		max	466.4	-44.2	44.5	266.9	110.5	490.0	602.2	506.4	616.6
		n	10	10	10	10	10	22	34	34	48

Table 4. Mass variations calculated for Au and related elements for the different lithological units. Gold, Se, S, Cu, Zn ans Pb mass variations are calculated using the Jowitt et al. (2012) method whereas As, Sb and Te mass variations are calculated using the Nesbitt (1979) method. Average volcanic section calculated assuming 93.5% background altered samples and 6.5% samples being affected by specific alterations. Sulphide-rich samples correspond to samples hosting sulphide veins or breccias.

Table 5

	Au	As	Sb	Se	Te	S	Cu	Zn	Pb
Δ %	-46.0	-27.2	-2.5	-26.7	13.7	-8.4	-9.6	-7.9	-44.4
σ (%)	11.5	5.4	0.5	5.7	5.7	0.7	1.6	0.5	6.3
Δ ppm	-1.9E-04	-0.02	-6.2E-04	-0.05	3.2E-03	-97.52	-8.83	-7.58	-0.15
σ (ppm)	4.9E-05	0.004	1.33E-04	0.01	1.4E-03	8.33	1.47	0.49	0.02
Mass (t)	**2.9**	**339**	**9.2**	**741**	**48**	**1.4E+06**	**1.3E+05**	**1.1E+05**	**2.3E+03**
σ (t)	0.7	66.7	2.0	157	20.1	1.2E+05	2.2E+04	7.2E+03	321

Table 5. Variations of Au and related elements mobilised by hydrothermal fluid circulation in the sheeted dyke complex and the plutonic complex. Median values of background altered samples from the sheeted dyke and plutonic comlexes are used for the calculation. Mass calculation is done using a hydrothermal cell volume of 5 km3 (3.9 km3 of sheeted dyke comlex and 1.1 km3 of plutonic complex) and a density of 2.97 g.cm-3 for the two units (Teagle et al. 2006).

Table 6

Deposit	Location	Tonnage	S	Cu	Zn	Pb	Au	As	Sb	Se	Te	References
		Mt	%	%	%	ppm	ppm	ppm	ppm	ppm	ppm	
TAG active mound*	MAR	3.8	42.1	2.1	0.6	72	0.5	43	2	14		Hannington et al. (1998); Petersen et al. (2000)
Galapagos Fossil Hydrothermal Field Zone A	GSC	1.5	45.7	4.7	0.8	100	0.08	136	5.6	498	2.4	Perfit et al. (1999)
Galapagos Fossil Hydrothermal Field Zone B	GSC		26.2	3.4	2.9	500	0.39	125	4	233	1.2	Perfit et al. (1999)
Bent Hill	JFR	9	32.1	0.48	4.8	477	0.27	78	22	43		Goodfellow and Franklin (1993)
Hydrothermal Field at 12°50'N EPR**	EPR	0.52	34.3	2.21	0.21	180	0.05	94		42		Hekinian and Fouquet (1985); Fouquet et al. (1988)
Large VMS at 12°43'N EPR***	EPR		36.4	0.765	2.33	277	0.19	130		52		Fouquet et al. (1996)
Average mafic VMS		1-5		4.3	11.7	0.2	1.2					Herzig and Hannington (1995)
Average mafic VMS (late phanerozoic)		3.3		2	1.1	100	1.7					Barrie and Hannington (1999)

Table 6. Examples of mafic VMS deposit composition in base metals, Au and related elements. MAR= Mid-Atlantic Ridge; GSC= Galapagos spreading centre; JFR= Juan de Fuca Ridge; Troodos= Troodos ophiolite. *S as sulphide from Hannington et al. (1998) and metal concentrations form Petersen et al. (2000). ** Median values of all data from Henkininan and Fouquet (1985) and Fouquet (1988). ***Tonnage calculated assuming a cone of 200 m in diameter and 70 m of height (Fouquet et al. 1996) and a density of 3 g.cm-3 (Henkininan and Fouquet 1985).

Click here to download Supplementary Material: Appendices.xlsx